Chem Soc Rev

Graphene-based nanomaterials for versatile imaging studies

Journal:	*Chemical Society Reviews*
Manuscript ID:	CS-REV-01-2015-000072.R1
Article Type:	Review Article
Date Submitted by the Author:	27-Feb-2015
Complete List of Authors:	Yoo, Je Min; Seoul National University, Chemistry Kang, Jin Hyoun; Seoul National University, Chemistry Hong, Byung Hee; Seoul National University, Chemistry

Chem Soc Rev

RSCPublishing

REVIEW ARTICLE

Graphene-based nanomaterials for versatile imaging studies

Cite this: DOI: 10.1039/x0xx00000x

Je Min Yoo†, Jin Hyoun Kang†, and Byung Hee Hong*

Received 00th January 2012,
Accepted 00th January 2012

DOI: 10.1039/x0xx00000x

www.rsc.org/

Over the last decade, interests in graphene have surged for its unprecedented physical, chemical, electrical, and mechanical properties. In recent years, researchers' interests have gradually shifted to other notable properties of graphene – its environment-friendly nature with outstanding optical properties. Thus, graphene is considered to be a promising and attractive candidate for various biomedical applications such as NIR-responsive cancer therapy and fluorescent bio-imaging. To that end, appropriate preparations and novel approaches to utilize graphene-based materials such as graphene oxides (GOs), reduced graphene oxides (rGOs), and graphene quantum dots (GQDs) in biology and medical science are gaining growing interest. In this review, we highlight recent applications of graphene-based materials as novel prospects for versatile imaging studies with a brief perspective on their future applications.

1. Introduction

Since its first serendipitous, yet historical discovery by British scientists in 2004,[1] graphene has attracted significant attention of researchers from all fields of science for exploiting many of its exceptional properties. One of the major research foci have been replacing indium tin oxide (ITO) with large-scale, high-quality chemical vapor deposition (CVD) graphene for macroscopic applications such as flexible thin films for transparent electrodes. Additional studies in the fields of electronics, physics, and materials science have also been extensively investigated.[2]

Recently, given an increasing consensus on graphene's environment-friendly aspects, researchers have considered employing graphene in other branches of science such as biology and medicine. Researchers have primarily focused on utilizing the ability of graphene oxides (GOs) to quench fluorescence and the availability of their functional groups for molecular conjugation for various optical bio-sensing studies. In 2009, Lu *et al*. successfully detected fluorophore-labeled DNA on/off the basal plane of GOs.[3] This work was followed by detecting other small molecules such as phosphate containing metabolites, protein kinases, trypsin and neurotrans-

Je Min Yoo

Je Min Yoo was born in Seoul, Republic of Korea in 1989. He received his B.A degree in chemistry from Johns Hopkins University in 2012. Then he joined prof. Byung Hee Hong's Graphene Research Laboratory (GRL) to pursue his Ph.D degree in physical chemistry. His current research interests are focused on the applications of graphene-based materials in biomedicine which include graphene-based drug delivery and drug design.

Jin Hyoun Kang

Jin Hyoun Kang was born in Seoul and received his B.S degree in chemistry from Seoul National University in 2013. He joined prof. Byung Hee Hong's Group in 2013. He is currently pursuing his Ph.D degree in physical chemistry. His current research interests are focused on the optical phenomenon and device applications of 2-dimensional materials.

-mitters with appropriate surface modulations.[4-7] A recent report by Mei *et al*. illustrated that logically designed GOs gates could discriminate Fe^{3+} and Fe^{2+} in living cells by exploiting the difference in fluorescence quenching.[8] Some researchers devoted special attention to unusual characteristics of stem cell growth and differentiation on graphene film substrates, which could possibly open new venues in stem cell engineering.[9,10] Moreover, high optical absorbance of GOs, reduced graphene oxides (rGOs) and graphene quantum dots (GQDs) in the near-infrared (NIR) region facilitates selective photothermal/photodynamic applications, making graphene a promising versatile therapeutic tool. In particular, researchers have proved that malignant tumor cells can be directly ablated using NIR-responsive photothermal therapy.[11,12] Graphene-based materials have also been employed to assist various photodynamic therapies, some showing the possibility of combining graphene-based photodynamic agents with either photothermal therapies or chemotherapies.[13-15] Other studies have utilized graphene hyperthermia as an external cue for efficient and controlled gene/drug delivery either by disrupting endosome or drug containing matrix.[16-18]

In addition to the studies discussed above, dispersed graphene derivatives are known to exhibit outstanding characteristics suitable for versatile imaging applications. Although technical breakthroughs in science have yielded different ways for appreciating diverse cellular/subcellular events on highly sophisticated levels, the real-time imaging with adequately high temporal and spatial resolutions still remains quite challenging in many aspects. At the same time, developing effective and stable fluorescent probes has been and continues to be one of the most important tasks in fluorescence bio-imaging. Likewise, other imaging tools such as Raman spectroscopy, which exploits scattered light derived from vibrational excitation mode of molecules, requires adequate imaging agents for generating clear and sharp signals. By the virtue of the unique properties of graphene-based materials, they are becoming gradually spotlighted as versatile imaging tools for assisting in both optical and non-optical imaging studies. Our goal here is to review the status of current research on graphene-based imaging studies, and discuss the perspectives for future applications.

Byung Hee Hong

Byung Hee Hong received B.S. (1998), M.S. (2000) and Ph.D. (2002) degrees in chemistry from Pohang University of Science and Technology. After spending 3.5 years as a post-doc at Columbia University (Advisor: Philip Kim), he joined the Department of Chemistry at Sungkyunkwan University as an assistant professor in 2007. Now he is an associate professor in the Department of Chemistry at Seoul National University.

2. Optical properties of graphene derivatives

2.1 Photoluminescence of graphene

Intrinsic graphene sheet with infinitely large sp^2 domains is not photoluminescent owing to its zero bandgap energy. To obtain photoluminescent graphene, various methods have been suggested for creating the bandgap by tailoring π electronic structures. Producing small particles by oxidative cutting of graphene, generating tiny sp^2 domains by plasma etching or tuning local electronic structures by chemical modifications all successfully manipulate the electronic structure of graphene sheets.[19-21] As have been extensively reported, the mechanisms of photoluminescence in graphene derivatives are not completely understood. While the exact mechanisms of photoluminescence are debated, experimental observations and theoretical calculations imply two possible mechanisms. One relates to the band-gap transition, as prevalently occurs in many semiconductor systems, while the other pertains to the electron-hole recombination relevant to the presence of defects. Eda *et al*. demonstrated that partial reduction of GOs enhances blue photoluminescence.[22] In that study, early (~3 min) exposure of GOs to hydrazine (N_2H_4) vapor enhanced photoluminescence around 390 nm, while further exposure rather reduced the intensity. Energy gaps of sp^2 domains depend on the domain size as described by the time-dependent density functional theory (TD-DFT), the energy of sp^2 domain composed of 20 aromatic rings yields blue photoluminescence above 2 eV (Fig. 1a). Theoretical calculations and experimental measurements indicate that a slight reduction of GOs generates nanosize sp^2 domains in GOs, yielding blue photoluminescence, and additional reduction causes merging of the sp^2 domains, which reduces the photoluminescence intensity. On the other hand, series of works demonstrated that the chemical modifications of graphene indicate that photoluminescence is not only related to the sp^2 domain sizes, but is also affected by the changes in local electronic structure that are induced by defects. Tetsuka *et al*. demonstrated simultaneous extraction of GQDs from GO sheets and modification of GQDs edges by primary amines.[23] Amino-hydrothermal treatment in ammonia solution at low temperature effectively cut out the small sp^2 domains embedded in the GO sheets, and concurrently primary amines bonded to the GQDs edges by ring-opening amination of epoxides. The photoluminescence wavelengths of GQDs are blue-shifted with gradually decreasing reaction temperature, implying that the higher amine density shifts the photoluminescence energy. The theoretical studies were performed using the density-functional theory (DFT) and TD-DFT calculations, which revealed that various edge modification strategies – heteroatoms doping, conjugation and even defects – yield the desired photoluminescence tuning (Fig. 1b).[24]

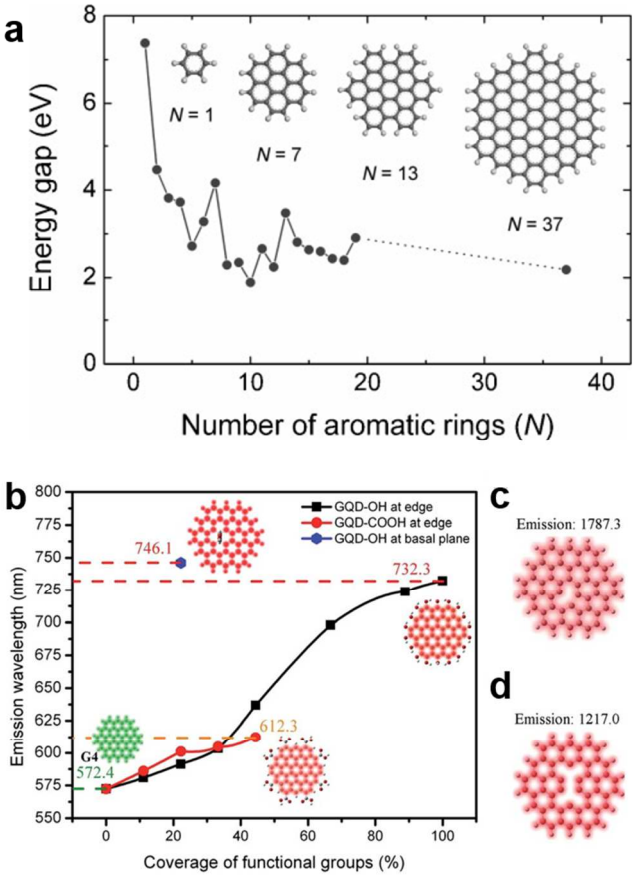

Figure 1 Theoretical photoluminescence of GQDs. (a) Energy gap of π–π* transitions calculated based on density functional theory (DFT) as a function of the number of fused aromatic rings. (b) Emission wavelength of oxidized GQD as a function of the coverage of –OH and –COOH groups. (c) and (d) are oxidized GQD with single or double vacancy defect, respectively. Reproduced from ref 22, copyright 2010 John Wiley & Sons; ref 24 with permission from The Royal Society of Chemistry.

Several reports measured the quantum yield (QY) of the synthesized GOs, and the reported QYs of GOs range from 0.02 % to 70.3 %.[25-28] In general, the synthesized GOs exhibit very low QY and sometimes even impossible to measure, but this could be enhanced by introducing simple chemical reactions. Slight reduction of GOs with hydrazine could readily produce a number of small sp^2 clusters in GOs, so the GOs would exhibit blue photoluminescence.[26] Functionalization with organic molecules also alters the optical properties of GOs. Q. Mei *et al*. demonstrated that amination of GOs by various alkylamines can increase the QY of GOs.[28] The sources of non-radiative electron-hole recombination sites (epoxide and carboxide) are covalently bonded and passivated by alkylamines during reaction, increasing the quantum yield from 0.02 % to as high as 13 %. While the QYs of GQDs are purportedly similar to those of GOs, recent reports indicate that GQDs show sufficiently high photoluminescence intensity for *in vivo/in vitro* imaging as we discuss in the later section.

2.2. Raman spectroscopy of graphene

Raman spectroscopy of graphene has been studied intensively, and become a standard tool for characterizing graphene. In bio-imaging, carbon nanotubes (CNTs) have been employed originally. Characteristic vibrational modes in CNTs, the radial breathing mode and the G band, are enhanced with electronic transition. However, because the electronic structure of CNTs is dependent on the chirality and diameter, the as-synthesized CNTs obtained through the chemical vapor deposition (CVD) methods show non-uniform properties. Unlike CNTs, graphene exhibits no chirality dependence in Raman scattering, and the electronic structure of graphene has a small band gap, allowing wide range of photons (visible to NIR) to be utilized in Raman spectroscopy.

Raman spectra of graphene display a few unique features, which are mostly characteristic vibrational modes in the 1000 cm^{-1} to 3000 cm^{-1} range: the D peak, the G peak, and the 2D peak.[29,30] The D peak at 1350 cm^{-1} corresponds to the breathing mode, similar to the one in CNTs but with higher frequency. The D peak intensity is determined by the density of defects, because the D peak is activated when defects are present. The 2D peak, often called the G′ peak, is located at around twice the frequency of the D peak. Whereas the D peak emerges as a result of the defects presence, owing to the momentum conservation between two phonons during scattering, the 2D peak is always observed in the spectrum. The G peak corresponds to the E_{2g} symmetry phonon modes, which reflect the in-plane motion of the carbon atoms. In dispersed graphene, such as GOs and functionalized GOs, the intrinsic defects and non-uniform structure yield intense and broadened D and G peaks, and attenuated 2D peak.[31] These peaks can be shifted by exploiting C13 isotopes, which assists exploring the mechanism of graphene synthesis and facilitating multicolor imaging in the case of CNTs. Among these, the G band is usually selected for bio-imaging to indicate the amount of graphene derivatives as the intensity of the 2D peak is low in oxidized graphene derivatives.

For practical imaging applications, the intensity of Raman scattering is crucial. Although the graphene derivatives usually show enough Raman scattering intensity without any treatment, it can be further enhanced by employing metal nanoparticles. Systematic study by Schedin *et al.* indicates that the array of Au nanoparticles enhances both of the G peak and the 2D peak intensities.[32] The enhancement of graphene peaks are mostly due to the surface plasmon resonance (SPR) effect and dipole effect of metal nanoparticles. Commonly used noble metals for surface enhanced Raman scattering (SERS), gold and silver effectively increase the Raman signals of graphene. These noble metal nanoparticles can be readily combined with or directly grown on GOs to enhance the characteristic peaks in graphene as demonstrated by the studies of Sun *et al*.[33] With 10 ~ 30 nm sized Au and Ag nanoparticles, the G peak showed 4-fold enhancement in the case of graphene/Au, and 13-fold increase for graphene/Ag (Fig. 2).

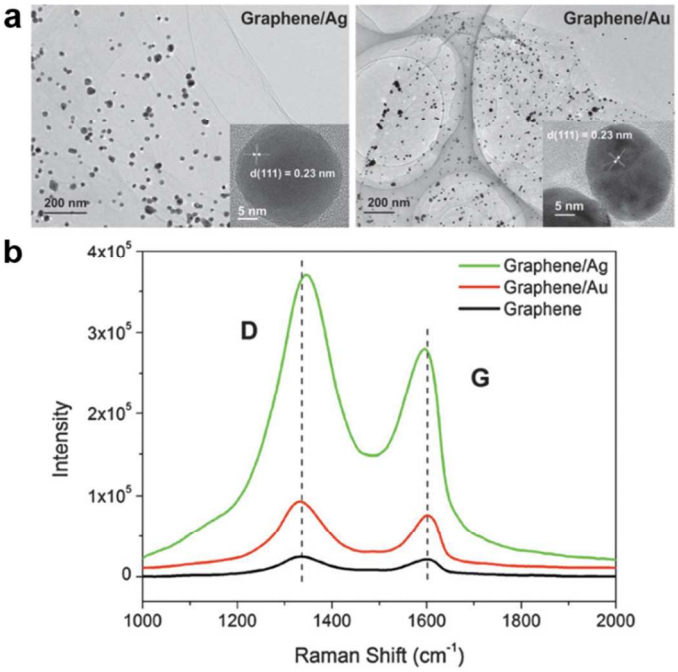

Figure 2 Raman signal enhancement of graphene using SERS. (a) TEM images of graphene/Au and graphene/Ag nanocomposites. The insets are the corresponding HRTEM images. (b) Raman spectra of graphene, graphene/Au and graphene/Ag nanocomposites in their aqueous dispersions. Reproduced from ref 33 with permission from the PCCP Owner Societies.

2.3 Photoacoustic wave generation by NIR light

Photoacoustic effect is the generation of an acoustic wave by the electromagnetic wave absorption. When pulsed electromagnetic wave (or light) is absorbed by a matter, a slight increase in the bulk temperature triggers expansion, resulting in pressure differences that generate the acoustic wave.[34] Several studies reported photoacoustic effects of graphene, mostly based on the photothermal effects induced by the NIR light. In general, the strength of a photothermal effect is proportional to the absorption cross-section of the incident laser. Photoacoustic effect is usually suppressed in GOs and GQDs, because the disconnected small sp^2 domains with oxygenated functional groups have higher transition energy between the highest occupied molecular orbital (HOMO) and the lowest unoccupied molecular orbital (LUMO) than the larger sp^2 domains, resulting in low NIR absorbance. When oxygenated graphene derivatives are reduced, small fragments of sp^2 domains are enlarged and connected, resulting lower energy transitions. rGOs, which usually are sufficiently reduced GOs with recovered electronic structure, can effectively absorb photons in the NIR range because of the large sp^2 domains.[35] The extinction coefficient of rGO at the NIR region is comparable to that of the single-walled CNTs (SWCNTs) and gold nanorods, which are commonly used photothermal or photoacoustic imaging agents.[11] In point of fact, several recent reports have demonstrated that rGOs can effectively generate photoacoustic effect using NIR light.

3. Preparation of Graphene for Imaging Applications

GOs and GQDs are widely employed in a number of biological applications due to the low cytotoxicity, large surface area and high dispersibility in various polar solvents. GOs are typically obtained through the Hummer's method while GQDs are prepared by thermo-oxidatively cut GOs or other carbon precursors. These graphene derivatives show outstanding optical properties, which make them suitable for versatile applications including bio-imaging. Table 1 summarizes the major features of graphene derivatives for bio-imaging. Simple modifications of GOs and GQDs make these graphene derivatives better prepared for specific imaging applications. The following section will briefly discuss about a few modification methods of graphene-based materials.

3.1 Enhancing the stability in physiological conditions

GOs can be dispersed in distilled water without much aggregation for several months, but are prone to aggregation in physiological solutions which commonly contain ionic salts. One of the strategies for enhancing stability in biological conditions is introducing biocompatible hydrophilic polymers and reducing the size of GOs. Although the synthesized GOs exhibit wide size distributions, the average size can be reduced by sonication. Many recent reports indicate the sonication assisted modifications reduce the average size of GOs owing to the high sonication energy, and large GO particles can be broken down into much smaller ones, as small as 10 nm.[36] Since small sized GOs show improved dispersion stability in polar solvents including physiological solution,[37] sub-500 nm GOs were commonly used in bio-imaging. For modification with hydrophilic polymers, polyethylene glycol (PEG) is one of the most preferably used polymers. Sun *et al.* grafted branched PEGs on GOs for enhancing the dispersion stability in biological buffers and further application as imaging agents.[36] In that study, PEGs were bonded to GOs through the reaction with epoxy and carboxylic acid groups achieving PEGylated nanosized GOs, which showed exceptional stability in phosphate buffered saline (PBS). Many studies used PEGs to achieve high stability even in solutions with high concentrations of salts (~10% NaCl).[38] Other biocompatible hydrophilic polymers such as polyamido amine (PAMAM), dextran (DEX) and poly-acrylic acid (PAA) also can be used as stabilizer by covalent modification methods.[39-41]

3.2 Graphene as nanocarriers

As discussed in the previous section, GOs themselves are not efficient photoluminescent probes owing to their low QY. In addition, micrometer-scale GOs are purportedly more toxic than nanometer-scale GQDs, and their size could also perturb biological environment in non-trivial manner. More detailed discussion on the toxicity of graphene-based materials will be followed in the toxicity section. However, a large surface area of GOs covered with oxygen-containing functional groups enables effective chemical modification with other imaging probes, including organic dyes and inorganic quantum dots.

Table 1 A Summary of characteristic features of graphene derivatives for bio-imaging

	Structure	Optical properties	Modification methods	Toxicity	Imaging applications
GOs	Micrometer to sub-10 nm size of few layers graphene. Disrupted sp^2 domains with hydrophilic oxygenated functional groups (epoxide, hydroxide, carboxide).	Intrinsic photoluminescence is emitted with UV excitation, and tunable emission wavelength is located at the range of UV-Vis.	Covalent modification by amide coupling, ring-opening amination, or slight reduction by chemical reduction methods. Non-covalent approaches also can be used.	Generally more toxic than GQDs. Cell-line dependent toxicity but no significant toxicity for both *in vitro* and *in vivo* levels at low doses. Presumably biodegradable.	Fluorescence imaging (intrinsic and extrinsic) Raman imaging Photoacoustic Imaging (extrinsic) MRI (extrinsic)
GQDs	Few nanometer (2~5 nm) spatial size ensures small sp^2 domain size, and oxygenated functional groups are present at edge and basal plane.	Intrinsic photoluminescence is emitted with UV excitation, and tunable emission wavelength is located at the range of UV-Vis.	Covalent modification by amide coupling or slight reduction by $NaBH_4$ tunes photoluminescence properties.	Generally non-toxic (up to 1 mg/ml). Readily excreted through both renal and fecal clearance. No significant toxicity based on both *in vitro* and *in vivo* studies.	Fluorescence imaging (intrinsic)
rGOs	Large connected sp^2 domains than GOs, with few hydrophilic functional groups	Strong photoluminescence quenching effect with enhanced absorption cross-section in NIR range.	Non-covalent approaches using hydrophobic interaction or π-π interaction	Purportedly more toxic than hydrophilic graphene derivatives. Not-readily biodegradable without functional groups.	Fluorescence imaging (extrinsic) Photoacoustic imaging (intrinsic) MRI(extrinsic)

Oxygenated graphene derivatives can be easily labeled with fluorescent organic molecules. Peng *et al*. reported fluorescein-labeled GOs for intracellular imaging agents.[42] Due to the fluorescence quenching effect of GOs, PEGs were grafted before the fluorescein labeling makes space between GOs and PEGs. Obtained fluorescein-labeled GOs were internalized and utilized for subsequent imaging without appreciable cytotoxicity. Similarly, Yang *et al*. labeled GOs with cyanine 7 (Cy7), which is a commonly used NIR fluorescent dye, and used them as *in vivo* imaging agents.[43] Both GO-PEG and GO-Cy7 conjugates were achieved through simple amide coupling, and fluorescence microscopy revealed that resulting fluorescence labeled GOs show low *in vivo* toxicity with efficient passive tumor targeting ability (Fig 3a-c).

Non-covalent approaches could also label imaging probes on graphene-based materials. In the work of Hu *et al.*, the authors incorporated inorganic quantum dots (QDs) on rGOs.[43] Amphiphilic poly(L-lysine) was adsorbed on rGOs via the hydrophobic interaction, and 11-mercaptoundecanoic acid (MUA) capped-CdSe/ZnS QDs were adsorbed on poly(L-lysine)-rGO through the electrostatic interactions (Fig 3d,e). Bovine serum albumin (BSA) capped-QDs were also grafted on polyethylenimine (PEI) adsorbed rGOs.[46] Both examples showed respectable intracellular imaging abilities without much cytotoxicity. The availability for various surface modifications of GOs also facilitates their targeting ability. GOs modified with PEGs display long-term stability, showing exceptional passive targeting by enhanced permeability and retention (EPR) effect.[45] On the other hand, active targeting is generally occurred via host-guest interactions. Folic acid is one of the most predominantly studied cancer cell targeting molecules as folate receptors are generally overexpressed on cancer cells. In virtue of the carboxyl groups and hydroxyl groups on the surface of GOs, folic acids can be covalently attached to the GOs through simple EDC coupling reaction.[46] Antibody-based active targeting, including Herceptin and transferrin, is another feasible option for graphene-based materials, since the amine groups at the end of protein chains can be readily coupled with the carboxyl groups on GOs via amide coupling reaction.[47-49] Other various targeting molecules such as hyaluronic acid,[50] β-cyclodextrin,[51] and endothelial tumor targeting agents including TRC105 and vascular endothelial growth factor (VEGF) have also been studied to test graphene-based active targeting imaging agents.[52,53] In general, these imaging agents were confirmed to successfully target tumor cells without apparent toxicity.

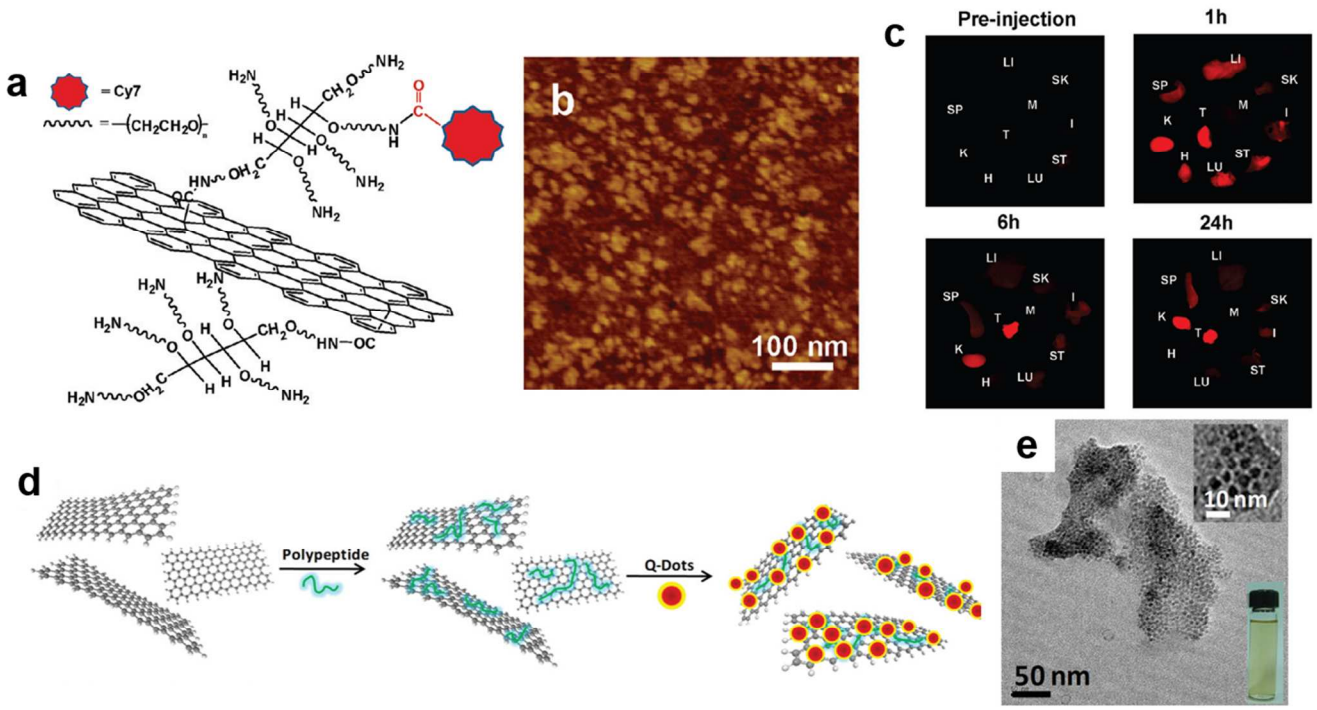

Figure 3 Covalent modification and Non-covalent modification of graphene. (a) A scheme of a nano-graphene sheet (NGS) with PEG functionalization and labelled by Cy7. (b) An AFM image of NGS-PEG. (c) Spectrally resolved ex vivo fluorescence images of organs before injection and 1, 6, and 24 h after injection of NGS-PEG-Cy7. (d) A scheme of sequential peptides and QDs adsorption on rGO sheets. (e) TEM image of the QD-rGO. Reprinted with permission from ref 43, copyright 2010 American Chemical Society; ref 46, copyright 2012 John Wiley & Sons.

3.3 Photoluminescent nano-GOs and GQDs

Although the intrinsic photoluminescence of GQDs is usually low, they can still be used as effective photoluminescent probes. Solvothermal fabrication methods generally yield GQDs with sizes ranging from 5 to 10 nm, and their corresponding QYs are typically below 20 %.[54-57] In 2011, Zhu *et al*. demonstrated the solvothermal synthesis of GQDs from GOs and bio-imaging for further applications[55] GOs prepared by the Hummers method were dissolved in DMF, followed by heating at 200°C using autoclave. This yielded GQDs with an average diameter of 5.3 nm, and green photoluminescence was observed with 11.4 % QY. Obtained GQDs were well-dispersed in polar solvents including cell culture medium, and incubation of MC3T3 cell with GQDs indicates cellular uptake of GQDs are occurred without considerable toxicity. Electrochemical methods can also be employed to obtain GQDs. Zhang *et al*. demonstrated that electrolysis of graphite produced water-soluble GQDs which could be used as imaging probes.[57] Electrochemical oxidation of graphite rod in alkaline condition produces homogeneous carbon solution, and further reduction with hydrazine results in green photoluminescent GQDs with 14 % QY. Different types of stem cells were clearly imaged using GQDs-based fluorescent probe, and the exhibited cytotoxicity was low.

Surface modifications can enhance the optical properties of GQDs. In 2012, Li *et al*. demonstrated microwave-assisted GQDs synthesis followed by subsequent reduction using $NaBH_4$.[58] In the study, initially synthesized greenish-yellow luminescent GQDs exhibited QY of about 11.7 %, and subsequently reduced blue luminescent GQDs yielded enhanced QY, reaching 22.9 %. Recently, Wu *et al*. reported GQDs with higher QY.[59] The authors' approach was bottom-up synthesis using L-glutamic acid as a precursor to produce hydrophilic nitrogen-doped GQDs. GQDs of about 5 nm and QY reaching 54.5 % were fabricated and effectively used in both *in vitro* and *in vivo* imaging. Zhu *et al*. demonstrated that chemical modification effectively alters the photoluminescence properties of GQDs.[60] Solvothermally produced GQDs can be reduced by $NaBH_4$ (r-GQDs) or grafted with alkylamines (m-GQDs). The emission wavelengths of both modified GQDs are blue-shifted, and the QYs are increased than pristine GQDs. Yet, both pristine GQDs and modified GQDs are successfully internalized and imaged without significant cytotoxicity.

3.4 Reduction of GOs

rGOs have been considered for photothermal therapy and photoacoustic imaging agents due to their high absorption cross-section in the NIR region. GOs can be reduced via photothermal,[27] electrochemical,[61] or chemical reduction,[62] but chemical reduction is considered as the easiest way to obtain rGOs. In 2007, Stankovich *et al*. demonstrated that hydrazine can reduce GOs dispersed in water.[62] Ever since, hydrazine has been widely used to produce rGOs. However, owing to the toxicity of hydrazine and insolubility of rGOs, further surface modifications have also been performed afterwards. Contrary to GOs, covalent surface modifications cannot drastically change

the properties of rGOs as only negligible amount of carboxyl and epoxy groups are present. Instead, non-covalent approaches using the π-π interaction between basal plane and aromatic molecules are used to modulate the surface properties of rGOs based on the strong van der Waals interaction. To obtain highly dispersible rGOs, PEGs terminated with hydrophobic alkyl chains can be attached, as suggested by the work of Shi *et al*.[63]

In recent years, various proteins are employed as a reducing agent and stabilizer of GOs for better biocompatibility and stability. Liu *et al.* demonstrated GOs can be reduced by gelatin and well-dispersed in physiological solutions.[64] Resulted gelatin-rGO nanosheets were also internalized in cells without considerable cytotoxicity, and used as effective *in vitro* imaging agents. Sheng *et al.* demonstrated that bovine serum albumin (BSA) can reduce GOs and simultaneously behave as a surfactant, producing hydrophilic rGOs which can be successfully used as *in vivo* imaging agents.[65]

4. Toxicity

4.1 Previous Issues Underlying the Toxicity of Imaging Agents.

Among several considerations pertaining to the imaging agents, toxicity is regarded as one of the most critical issues. Toxicity in biomedicine is associated with many different biological phenomena including the generation of harmful reactive oxygen species (ROS), membrane damage caused by physical puncture and molecular intercalation in DNA.[66-73] Additionally, some forms of toxicity observed *in vivo* are often correlated to reticuloendothelial system (RES) clearance, circulation time, hematological and histological factors, organ accumulation and subsequent damage.[53,74-78] Non-trivial toxicity caused by desired imaging agents not only poses difficulties related to the accurate collection *ex vivo* data, but also precludes their potential usage *in vivo* studies.

In the case of inorganic quantum dots (QDs), their exceptionally high fluorescence quantum yield (> 80 %, commercially available) and photostability have encouraged their universal applications as powerful fluorescent imaging agents. Nevertheless, the core structure of these QDs contains extremely toxic heavy metals such as cadmium. Although this issue still remains very controversial, several reports have discussed the cytotoxicity of QDs, which is generally attributed to the leakage of cadmium ions, cytotoxic ligands and sometimes to the self-aggregation tendency of QDs.[69-72,79,80] Some researchers are also concerned with the QDs size-related nanotoxicity that may alter some important biological functions and trafficking of the molecules of interest.[81]

In a similar manner, toxicity associated with carbon nanomaterials (CNMs) such as carbon nanotubes (CNTs), a rolled one-dimensional version of graphene sheets, has also been extensively investigated. Although the promising role of CNTs as imaging agents for Raman spectroscopy has been clearly demonstrated, multiple studies reported their potential harmful impacts on human health. These studies suggest that CNTs induce continuous generation of ROS with lethal outcomes including DNA damage and sometimes direct cell membrane puncture.[82-86] Despite the fact that observed toxicities and degradability are distinctive of the shape, size (i.e. single-walled or multi-walled) and degree of functionalization, further studies seem inevitable for qualifying the use of CNTs as imaging agents.[87-89]

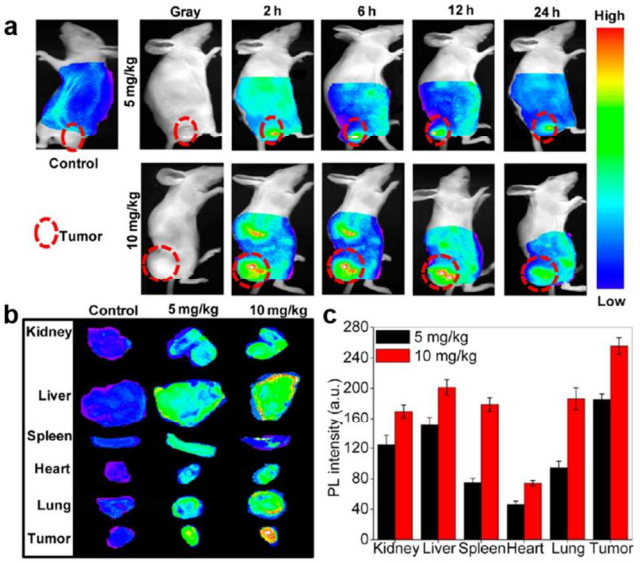

Figure 4 In vivo imaging and biodistribution of the carboxylated GQDs. (a) The in vivo imaging of KB tumor bearing mice after intravenous injection of GQDs (5 and 10 mg/kg). (b),(c) ex vivo images and quantitative distribution of isolated organs of mice at 24 h after injection. Reprinted with permission from ref 76, copyright 2013 American Chemical Society.

4.2 Toxicity of Graphene-based Materials.

Although CNTs and graphene-based materials are some of the most widely studied nanoscale sp^2 carbon allotropes with very similar chemical composition, recent studies have observed entirely different levels of toxicities from these two classes of materials.[90,91] Unlike CNTs, most studies have generally agreed on the negligible cytotoxicity of graphene-based materials.

4.2.1 *In vitro* Toxicity of Graphene-based Materials

Over the last few years, several groups investigated cellular internalization and *in vitro* cytotoxicity of functionalized graphene derivatives: GOs and GQDs using different types of mammalian cells. These reports generally confirmed low cytotoxicity and relatively high cellular uptake, which makes graphene-based materials suitable for various biomedical applications.[77,78,92-95] Nevertheless, some researchers argued that the cytotoxicity of a few hundred nano-meter or micro-meter sized GOs is much higher than that of GQDs, which should not be disregarded in biomedical applications.[78,94] In particular, some studies indicated that GOs and GOs-based nanoplatelets are related to severe cytotoxicity and lung diseases.[96,97] Other researchers revealed heterogeneous cell-specific cytotoxicity of GOs by performing cytotoxicity screening of GOs on multiple different cell lines.[98] In general, the cytotoxicity of graphene-based materials was found to be strongly related to the size of particles, which could partially

explain lower cytotoxicity of a few nano-meter sized GQDs over a few micro-meter sized GOs.[94,97,99] On the contrary, Akhavan *et al.*, have repeatedly argued that the cytotoxicity of graphene-based materials is independent of size, but direct interaction of the sharp edges of graphene with the cell membranes is more likely mechanisms underlying the observed cytotoxicity.[100,101] In other words, the authors believe that nanosized GOs can also be lethal to mammalian cells. Thus, detailed toxicity mechanisms pertaining to the size and shape of graphene-based materials are still uncertain and further studies seem unavoidable.

In addition, the effects of graphene functionalization in cell membrane permeability and cytotoxicity were studied by many researchers. The authors commonly discussed that covalently attaching hydrophilic molecules such as polyethylene glycol (PEG) to the edges of graphene enhances solubility and biocompatibility in biological environment.[36] Some authors investigated possible toxicity effects of the functional groups by modifying them with –COOH, NH_2, $CO\text{-}N(CH_3)_2$, and –PEG.[95,102] Quantitative data analysis showed no distinct toxicity changes among these GQDs variants, while the cell membrane permeability increased respectively in the order of –PEG, –OH, and $–NH_2$.[69] These results are encouraging for researchers who endeavor to employ modified graphene derivatives as they all exhibit very low cytotoxicity.[103] In 2011, Sasidharan *et al*. studied distinct behaviors between pristine / hydrophobic graphene and carboxylated / hydrophilic graphene in biological environments. Compare to pristine graphene, carboxylated graphene pacify hydrophobic interaction with cell membrane and associated toxic effects such as the deformation of cell membrane and increased intracellular ROS level and subsequent apoptosis.[92] Indeed, graphene functionalization plays vital role not only in cell-nanoparticle interactions, but also in enzyme-catalyzed biodegradation, which will be discussed in the later section.

4.2.2 *In vivo* Toxicity of Graphene-based Materials

Besides the *in vitro* toxicity studies addressed above, many authors have explored *in vivo* biodistribution and toxicology of graphene-based materials recently. In 2010, Yang *et al.* discussed the long-term *in vivo* pharmacokinetics and biodistribution of PEGylated ^{125}I-labeled nanographene sheets (NGS) with systemic toxicology examination.[75] The radioactivity levels of ^{125}I-NGS-PEG were measured in the blood and many different organs over time after intravenous injection. Overall, they found persistently decreased radioactivity levels of ^{125}I-NGS-PEG in most organs. They presumed that small NGS-PEG particles may be cleared out by renal or fecal excretion. The authors also investigated long-term *in vivo* toxicology over 3 months by carrying out blood biochemistry and hematology analysis. Mice injected with 20 mg/kg NGS-PEG were sacrificed at different periods of time, and all parameters from the blood biochemistry and hematological data did not indicate any appreciable toxicity. In 2013, the same group carried out *in vivo* biodistribution and toxicology studies of functionalized nano-GOs by

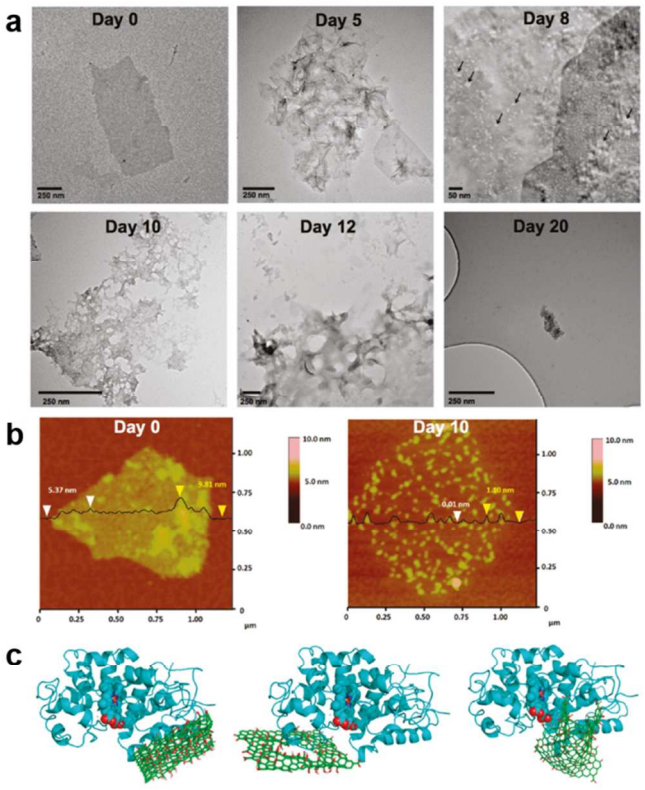

Figure 5 Enzymatic oxidation of GO. (a) TEM images of GOs incubated with horse radish peroxidase (HRP). (b) AFM images with GOs incubated with HRP. (c) Simulated docking between GO and HRP. Reprinted with permission from ref 104, copyright 2011 Americal Chemical Society.

administering it through two other major routes: oral feeding and intraperitoneal (i.p.) injection.[77] They revealed that oral administration induced no obvious tissue uptake, while i.p. injection led to high accumulation of nano-GOs in the RES system over a long periods of time. In spite of the results obtained through the i.p. injection, they found that both routes did not result in significant toxicity to the treated animals.

In 2014, Nurunnabi *et al.* reported *in vivo* biodistribution and toxicity of carboxylated GQDs by intravenously injecting them into mice.[76] The accumulation and potential toxicity were tested by performing a long-term serum biochemical analysis and histological evaluations. Overall, the study revealed no serious *in vivo* toxicity and GQDs were mainly found in the liver, spleen, lung, kidney, and tumor sites (Fig. 4). Further study confirmed that GQDs did not yield any appreciable organ damage or lesions in mice that were treated with GQDs by administering 5 mg/kg or 10 mg/kg dosages for 21 days. These results were followed by similar conclusions of *in vivo* bio-distribution studies, illustrating fast clearance of GQDs from kidneys without significant accumulation in main organs.[98] Results of these biocompatibility studies suggest that GQDs can be used in clinical applications in the near future. However, these results also indicate that high doses of GOs can be toxic and have lethal outcome, on good agreement with the results of *in vitro* studies.

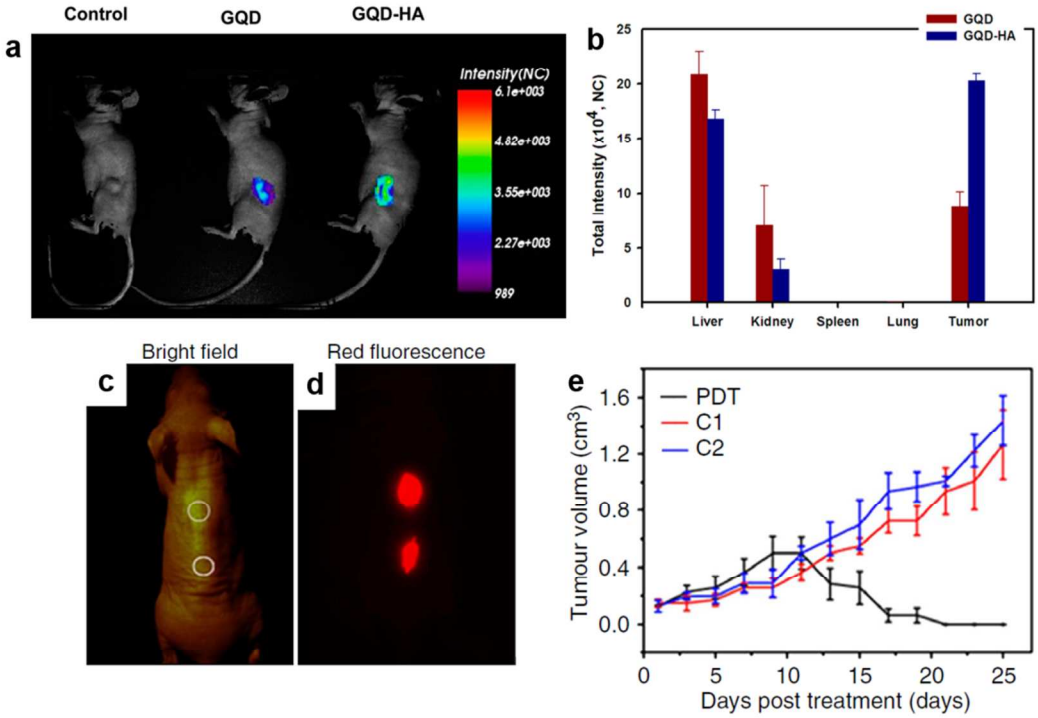

Figure 6 Graphene based in vivo targeting imaging agents. (a) In vivo fluorescence images of GQD-HA in mice after tail vein ingection. (b) Fluorescence intensity from dissected organs. (c),(d) Bright field image and in vivo fluorescence image after GQDs injection. (e) Time-dependent tumor growth curves. Reprinted with permission from ref 106, copyright 2013 American Chemical Society; ref 107, copyright 2014 Nature Publishing Group.

4.2.3 Biodegradation of Graphene-based Materials

As much as various parameters of *in vitro* and *in vivo* toxicity studies are important, thorough understandings on oxidation/biodegradation processes of graphene-based materials are crucial for universal and beneficial applications. In 2011, Kotchey *et al.* reported enzyme-catalyzed oxidation of GOs and rGO by incubating each solution with low concentrations of hydrogen peroxide and horseradish peroxidase (HRP).[104] Strikingly, the study revealed that the degree of functionalization is directly correlated with the degree of enzyme-catalyzed oxidation. Results from Raman spectroscopy, transmission electron microscopy (TEM) and atomic force microscopy (AFM) confirmed that mild enzymatic oxidation with HRP induced the formation of holey graphene oxide, which eventually resulted in fully oxidized debris of GOs flakes (Fig. 5). On the other hand, incubation of rGOs with HRP did not make any significant changes in terms of enzymatic oxidation. The authors deduced that the presence of functional groups on GOs induced looser binding with HRP and allowed the enzyme to be more dynamic; the catalytic heme site of HRP was thus brought in proximity of GOs. On the other hand, more hydrophobic rGOs made tighter binding with HRP without making contacts with the catalytic heme site. In 2012, the same group reported thorough investigation on the enzyme-catalyzed degradation of CNMs using HRP and myeloperoxidase (MPO).[87] The report verified promising aspects of functionalized CNMs for *in vivo* applications as they are presumably biodegradable by intracellular enzymes with peroxidase activity such as human MPO (hMPO). Nevertheless, it should be noted that the experimental results are not directly correlated with actual biodegradation in the human body as the physiological hMPO levels are generally more diluted than the experimental conditions. In addition, the oxidative debris of GOs nanoflakes could be another possible source of toxicity.

5. Optics-based Imaging

5.1 Fluorescence Bio-imaging

For practical fluorescence imaging studies, a fluorescent probe should satisfy certain conditions.[105] Foremost, it should be readily excitable with sufficiently high quantum yield. Fluorescence intensity and quantum yield are important for minimizing fluorescent probe-based toxicity and radiation damage by the incident laser light while maximizing the fluorescence emission. In addition, the probe should be sufficiently resistant for maintaining the original properties through long-term arrest in biological fluids without blinking and photobleaching. A fluorophore should not exhibit considerable cytotoxicity and it is desirable to have functional groups available for conjugation with other molecules to effectively target specific objects of interest. In the process of such developments, numerous novel candidates, such as green fluorescent proteins (GFPs) and inorganic quantum dots were designed and proposed to be the 'ideal' fluorescent probes.[66,105]

Nevertheless, these probes have a few drawbacks that limit their universal applicability such as photobleaching and considerable cytotoxicity.

Recently, researchers have suggested graphene derivatives as a new class of fluorescent probes for biomedical imaging due to their unprecedented characteristics. Photoluminescent GQDs have been employed for various fluorescence imaging applications. Researchers take advantage of photostable, non-toxic and easily conjugatable GQDs for versatile applications which include *in situ* drug delivery imaging. In this section, we will skip the basics of fluorescence cell imaging studies by graphene derivatives and will highlight some noticeable applications.

5.1.1 Tracking targeted drug / gene delivery.

Numerous drug delivery strategies and direct photothermal ablation of tumor cells have been accompanied by various graphene-based platforms. Although many of these studies performed *in situ* imaging of drug delivery/therapy, most of these studies utilized coated inorganic quantum dots and other fluorescence molecules attached to graphene-based materials to visualize the phenomena. In 2013, Nahain *et al.* presented two graphene-based anti-cancer drug delivery methods using rGOs and GQDs.[50,106] In the case of rGO-hyaluronic acid (HA) conjugate system (avg. size ≅ 200 nm), spiropyran was additionally attached as a photochromic dye for yielding graphene-based fluorescent nanocomposite.[50] It should be noted that these authors repeated similar experiments without attaching additional fluorescent materials. Instead, they utilized the intrinsic fluorescence of GQDs with an average size of 20 nm to confirm efficient targeting of GQD-HA to desired receptors.[106] Successful delivery of GQD-HA conjugate to overexpressed CD44 receptors was confirmed by obtaining fluorescence images from the tumor tissue through both *in vitro* and *in vivo* observations (Fig. 6). Anti-cancer treatment was subsequently administered by releasing doxorubicin under mildly acidic conditions, which was loaded onto the basal plane of GQDs. Although previously studied graphene-based therapy/imaging applications included other fluorescent molecules, researchers endeavor to exploit the luminescence of GQDs for *in situ* therapy monitoring. In 2014, Ge *et al.* incorporated a few nano-meter scale GQDs in highly efficient photodynamic cancer therapy with simultaneous fluorescence imaging.[107] In this study, the authors successfully synthesized GQDs with a broad absorption spectrum and strong deep-red emission peaking at 680 nm. Through both *in vitro* and *in vivo* experiments, the authors clearly demonstrated that GQDs can be considered as promising PDT agents, with superior singlet oxygen quantum yield, photo- and pH-stability and even simultaneous fluorescent imaging.

5.1.2 Tracking targeted proteins.

While most researchers have focused on exploiting GQDs' fluorescence for monitoring *in situ* drug delivery to confirm successful targeting, Zheng *et al.* demonstrated that GQDs can be utilized as universal fluorophores that could reveal some important biological functions (Fig. 7).[81] In this study, specific labeling and dynamic tracking of insulin receptors were achieved through GQDs fluorescence of internalized and recycled insulin receptors in adipocytes. The authors tried to determine the specific functions of some relative proteins. By dynamically tracking the insulin receptors, the authors found that the internalization and recycling of insulin receptors are oppositely regulated by two distinct proteins: 1) apelin, which improves the insulin sensitivity, and 2) TNFα, which enhances the insulin resistance. Although this study alone did not fundamentally change the therapeutic approaches to diabetes treatment, divulging important cellular/subcellular functions revealed by using the GQDs fluorescence would be helpful for various future biomedical studies.

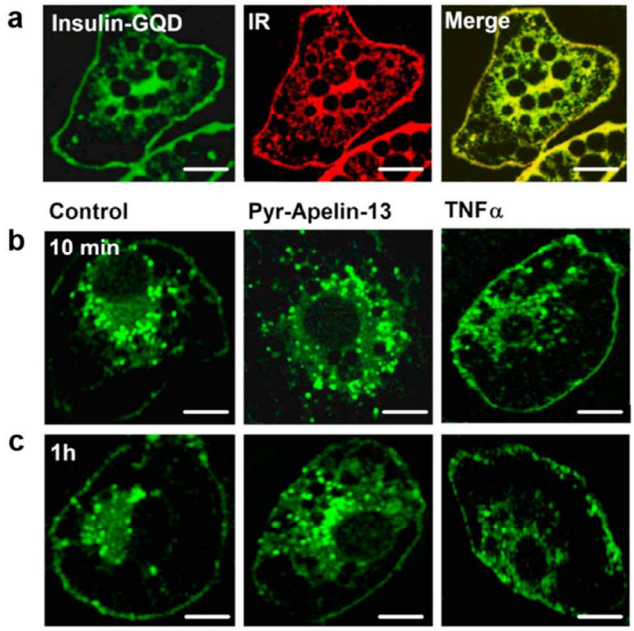

Figure 7 Dynamic tracking of protein of interest. (a) Confocal fluorescence images of insulin conjugated GQDs (green, left) or with antibodies against insulin receptor (IR) (red, middle). (b),(c) Cellular distribution of insulin receptors after (b) 10 min or (c) 1 h incubation with insulin-GQDs. Scale bar = 10 μm. Reprinted with permission from ref 81, copyright 2013 American Chemical Society.

5.1.3 Multi-photon imaging techniques.

Current imaging strategies mostly utilize fluorescent molecules, including GQDs, with UV-vis emission (generally 400-600 nm). For non-invasive analysis, however, longer wavelength imaging studies are preferred as they not only provide less damaging analysis methods but also enable deep tissue imaging. For such reasons, NIR-emitted fluorescent probes are attracting increasing attention and attempts exist for synthesizing GQDs with NIR fluorescence emission. However, these approaches often cause difficulties for various reasons and multi-photon imaging is considered to be a great alternative. Indeed, bright multi-photon fluorescent probes can provide more detailed analysis of various cellular/subcellular activities in deep region of biological samples with larger imaging depth, weaker photo-induced damage and minor autofluorescence background.[108,109]

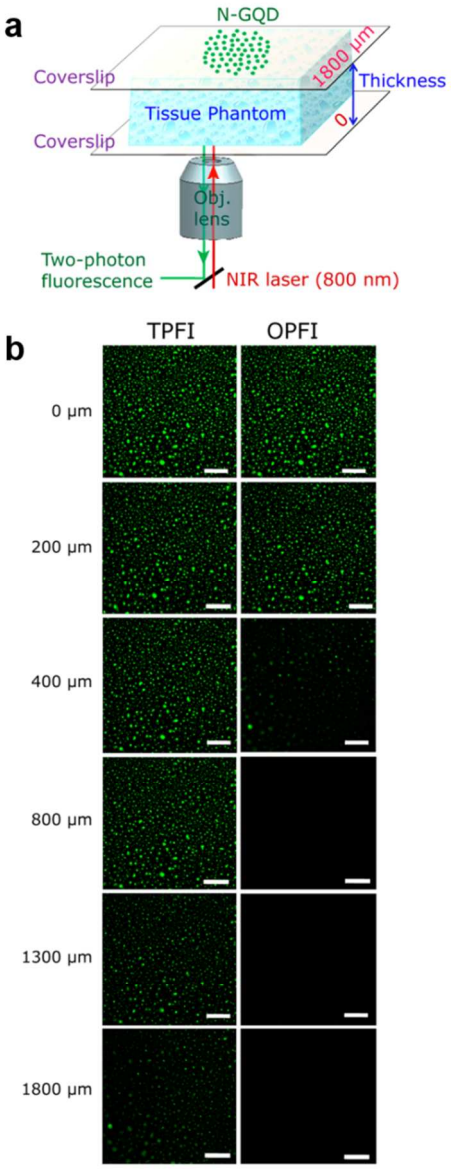

Figure 8 Two-photon fluorescence deep tissue imaging. (a) Schematic of the measurement setup. (b) Penetration depth of N-GQDs for TPFI (two-photon fluorescence imaging) and OPFI (one-photon fluorescence imaging) in tissue phantom. Reprinted with permission from ref 109, copyright 2013 American Chemical Society.

On the other hand, multi-photon imaging, which utilizes two or more number of lower energy photons to excite a fluorophore in a single quantum event, exhibits a few primary advantages over one-photon imaging. Foremost, the nonlinear excitation mode generates relatively high levels of spatial resolution, with only the desired region can be readily excited with lower chance for photobleaching events. More importantly, multi-photon excitation is purportedly well-suitable to image deep-range tissues as two-photon excitation wavelength is known to be in the range of 700–1350 nm. In 2012, Qian *et al.* reported two-photon and three-photon induced *in vitro* and *in vivo* cell imaging of PEG-GO nanoparticles with an average size of about 40 nm.[108] In that study, the three-dimensional distribution of fluorescent PEG-GO nanoparticles was clearly visualized even for deep tissue imaging. This report was followed by a similar two-photon study by Gong *et al*. In the report, the authors utilized ultrasmall sized nitrogen-doped GQDs (N-GQDs) as a biocompatible and photostable fluorescent probe for deep tissue cellular imaging (Fig. 8).[109] According to the results, the cross-section of N-GQDs exhibited two-photon absorption of around 48000 Goppert Mayer units, which significantly exceeded that of conventional organic fluorophores. More remarkably, the penetration imaging depth of N-GQDs was still considerable (as deep as 1800 μm), which can be clearly observed from the figure. As demonstrated from the preceding studies on multi-photon cellular imaging with GQDs and other graphene derivatives with exceptional photostability and non-toxicity, these materials are very promising candidates for non-invasive bio-imaging probes to be designed in the near future.

5.2 Raman imaging

Fluorescence microscopy is the most common bio-imaging technique, but high excitation energy, photo-bleaching, and broad excitation/emission peak widths are some of its drawbacks. By contrast, Raman spectroscopy exploits scattered light derived from molecular vibrational excitation modes. Thus, the photon energy does not need to match the electronic excitation energy, and lower energy of incident laser light can be used for assessing the biological samples without inflicting significant damage. In addition, reduced photo-bleaching and narrow peak width yield more stable and multiplex observations.[110-112] However, the low efficiency of Raman scattering precludes it from becoming a universal imaging technique. One of the breakthroughs is introduction of high-resolution EM-CCDs, but this is economically unfavorable. Up to date, promising Raman imaging techniques have been developed for bio-imaging applications, including surface-enhanced Raman scattering (SERS) which solved the efficiency issue to some extent.[113,114]

5.2.1 Metal particle decoration for SERS imaging

Unlike small organic molecules, GOs exhibit intrinsically strong D and G peaks without any enhancements. The Raman peaks of graphene can be further enhanced by depositing metal nanoparticles as we discussed in the earlier section. Several works addressed direct growth of nanoparticles on hydrophilic GOs. Namely, gold nanoparticles and silver nanoparticles were decorated on GOs using citrate,[33] PVP,[115] and DMF[116] as reducing agents. Besides the direct growth, synthesized nanoparticles could also be readily combined with GOs.[117]

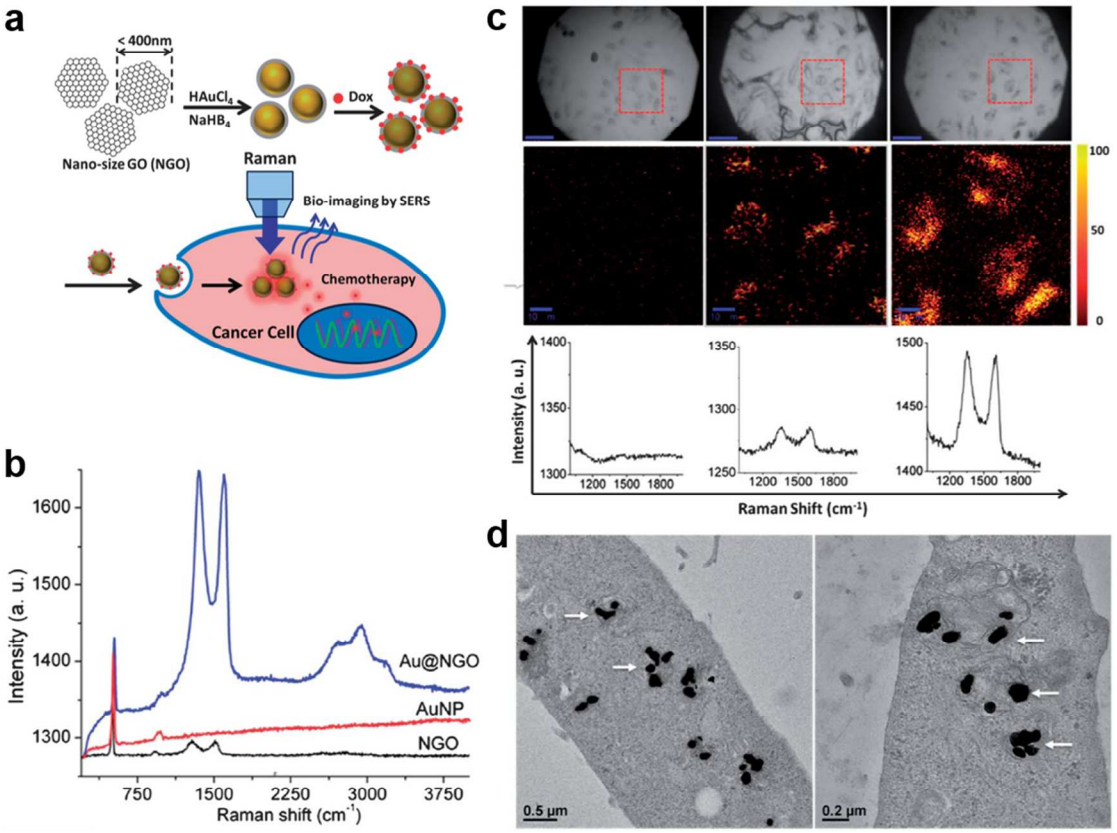

Figure 9 In vitro Raman imaging using SERS effect. (a) Schematic diagram of Au nanoparticle-GO (Au@NGO) synthesis. (b) Raman spectra of Au@NGO and both bare materials (AuNP and NGO). (c) In vitro Raman imaging of HeLa cells. (d) TEM images of HeLa cells incubated with Au@NGO. Reproduced from ref. 120 with permission from The Royal Society of Chemistry.

Liu *et al.* used directly grown Au-graphene oxide composite, which exhibited remarkably enhanced D and G peaks under 632.8 nm laser illumination.[118] Irradiation damage to cells induced by long acquisition time and strong irradiation power can be suppressed with highly sensitive SERS effect of Au on the GOs surface. Reduction of $AuCl_4^-$ by citrate produces an average of 20 nm Au nanoparticles on GOs, which are mostly under 400 nm in size. Raman imaging of HeLa 229 cells incubated with Au nanoparticle-decorated GO composites (Au-GO) disclosed the cellular uptake mechanisms of Au-GO. In contrast to the incubation at 37 °C, the intracellular Raman signals of Au-GO composites were not detected upon incubation at 4 °C. The result suggests the cell internalization of Au-GO composites takes place by ATP-dependent endocytosis. In a similar study by Huang *et al.,* the authors synthesized an Au-GO composite via post-addition of gold nanoparticles to GOs solution. Au nanoparticles with an average size of 20 nm were decorated on sub-200 nm GOs through amide coupling between PEG and DMSA ligands on Au particles, and were utilized as Raman imaging probes for studying cellular uptake mechanisms in Ca Ski cell line due to the enhanced signal intensity.[119] Treatments with inhibitors, methyl-β-cyclo dextrin (MβCD) and NaN_3, suggest the cellular uptake of GOs would be clathrin-mediated endocytosis.

Recently, Ma *et al*. reported gold nanoparticles compactly wrapped within nanosize GOs (NGO) as Raman imaging probes for drug delivery system.[120] $HAuCl_4$ was added to the solution of NGO, sonicated and reduced by using mild reducing agent, $NaBH_4$. This process resulted in the formation of NGO-encapsulated Au nanoparticles (Au@NGOs) with an average size of about 100 nm. The D and G peaks of Au@NGOs were about one order of magnitude stronger than those of the NGO, revealing sensitive imaging of internalized Au@NGOs in HeLa cells (Fig. 9). Besides the passive targeting of GO-based nanostructures, SERS-enhanced imaging probe can be used to actively target cancer cells by coupling folic acid (FA) with silver nanoparticle-decorated GOs, which is similar to the work reported by Liu *et al.* in 2013.[121]

6. Non-optics based imaging

6.1 Photoacoustic imaging

Optical imaging can be used for achieving high resolution images using techniques such as confocal microscopy and two-photon microscopy. However, optics-based imaging techniques in the visible range suffer from low penetration depth owing to the high scattering rates of light on tissues, limiting the

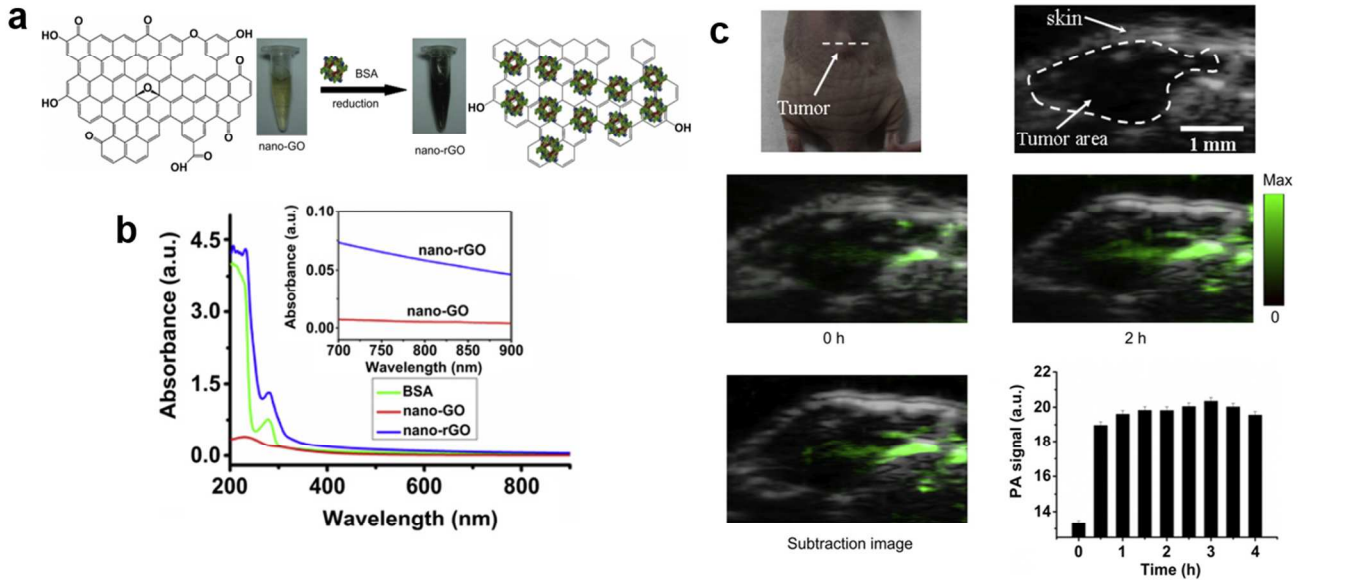

Figure 10 In vivo photoacoutic imaging using graphene based material. (a) Schematic of soluble rGOs preparation from GOs using BSA. (b) UV-Vis spectra of nano-GO and reduced form, nano-rGO. (c) photoacoustic imaging of tumor region in mice using nano-rGO as a photoacoustic contrast agent. Graph at the bottom right is PA signal as a function of the injection time. Reprinted with permission from ref 65, copyright 2013 Elsevier.

measurements that can be performed on the tissue surface.[122] On the other hand, low-energy electromagnetic waves can penetrate deeper than the short wavelengths. Radio frequency waves and/or ultrasound waves exhibit much lower scattering in the biological samples; thus, these waves can be suitable for deep tissue imaging.[123]

Although photoacoustic imaging has a promising potential, the photoacoustic signals of pathological tissues are frequently indistinguishable from normal tissues.[124] For effective diagnosis, proper photoacoustic contrasts are needed for enhancing the images of specific targets with lower energy excitation lasers. Early on, gold nano-clusters and/or optical contrasts were used as contrast agents in photoacoustic imaging for enhancing absorption cross-section in the NIR region.[125,126] Although several organic contrast materials have absorption peaks in the NIR region, photo-bleaching and fixed absorption peaks of organic molecules are the limitations precluding their wide use.

In 2008, Gambhir's group reported *in vivo* photoacoustic imaging using SWCNTs, opening new venues for CNMs as novel photoacoustic contrast agents.[124] In the case of graphene, photoacoustic imaging remains relatively unexplored. Because the absorbance in the NIR region is much weaker in GOs than that of CNTs, the photoacoustic wave generation is usually weaker. However, the dispersed forms of graphene can be produced more easily than CNTs; graphene has some economical advantages. In addition, high density of edge-functional groups enables chemical tenability, and reduced GOs leads to higher NIR absorbance. Recent studies on photoacoustic imaging with graphene focused on enhancing the absorbance in the NIR region.

6.1.1 Composite approaches

Indocyanine green (ICG), which efficiently absorbs light in the NIR region, is used as an assistant for enhancing the absorption cross-section for NIR laser.[127] By coupling the GO of ~ 200 nm and ICG through simple mixing, the resulting composite exhibits enhanced absorption in NIR region. Additionally, folic acid can be coupled to target tumor cells such as the HeLa cell. The resulting photoacoustic image clearly demonstrated the targeting ability of these graphene-based contrast agents. Although GO coupled solely with ICG (ICG-GO) or folic acid (GO-FA) could not be used for efficient imaging of the tumor cells, coupling with both (ICG-GO-FA) clearly demonstrated the HeLa cell targeting and imaging ability, illustrating the promising aspect of graphene-based photoacoustic agents.

6.1.2 Photoacoustic imaging with rGO

The photoacoustic effect is usually suppressed in GOs owing to the low absorbance in the NIR region. The disconnected small sp^2 domains with oxygenated functional groups have higher transition energy between HOMO and LUMO than the larger sp^2 domains. rGOs, with larger sp2 domains than GOs, can absorb NIR light more efficiently, but their poor solubility precludes from being used as imaging agents. In 2012, Liu's group solvothermally reduced GOs simultaneously with decorating magnetic iron oxide nanoparticle (IONP), followed by conjugation with PEGs for solubility enhancement.[128] After the solvothemal reduction and PEGylation, the size of composite is reduced down to 50 nm. The rGO composite exhibited enhanced absorption of NIR light and intravenously injected rGO-IONP composite accumulated at tumor sites, generating strong photoacoustic signals. Besides

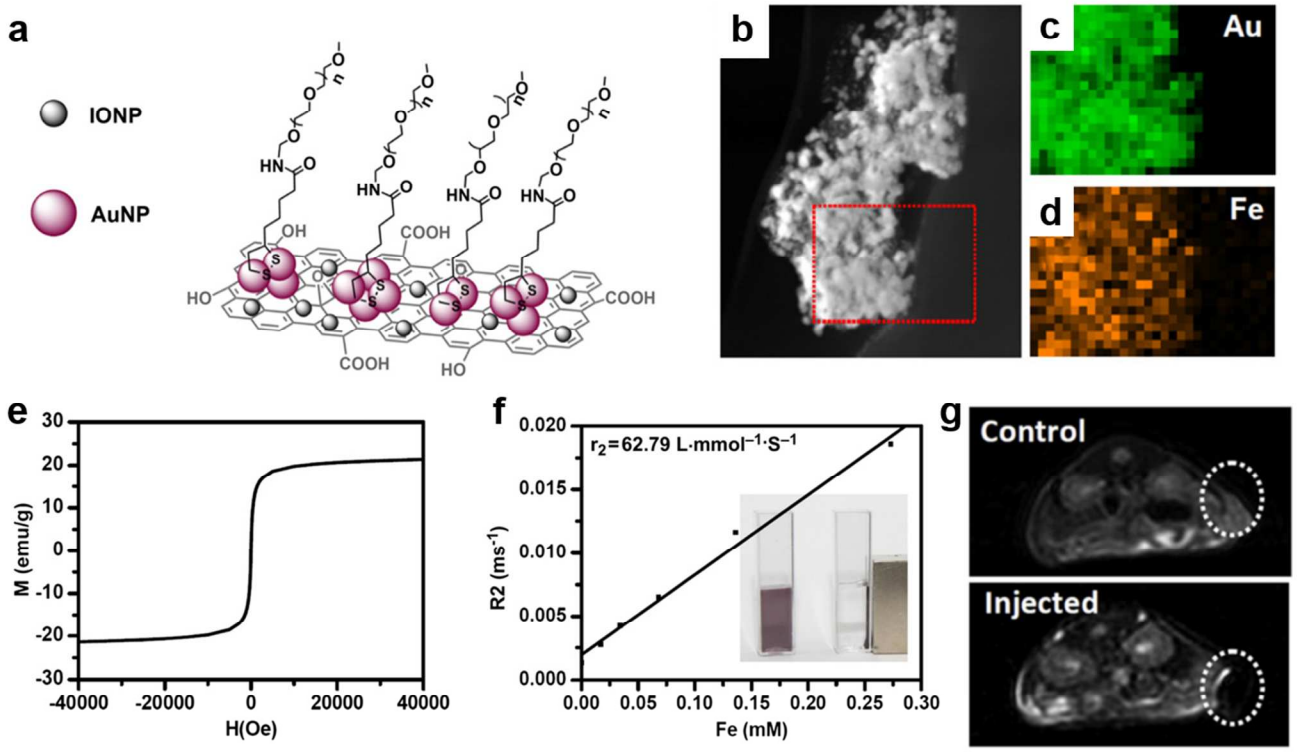

Figure 11 Graphene based MRI imaging. (a) Schematic representation of paramagnetic nanoparticle coordinated GO (GO-IONP-Au). (b) Scanning tunnelling electron microscope (STEM) image, and (c),(d) energy dispersive X-ray spectroscopy (EDS) images of GO-IONP-Au. (e) Magnetization loops, and (f) T_2 relaxation rates with Fe concentration. (g) T_2-weighted magnetic resonance images of 4T1 tumor-bearing mice before and after intratumoral injection of graphene based contrast agent. Reprinted with permission from ref 137, copyright 2013 Elsevier.

the two-step reduction and stabilization, GOs can be reduced and stabilized by one-step reduction using BSA, as reported by Sheng et al.[65] BSA effectively reduced nano-GO, and obtained nano-rGO shows an average size of 70 nm, and the UV-Vis absorption spectrum indicates around 5-fold increase of NIR absorption (700-900 nm). Owing to the high NIR absorbance, tumor was successfully imaged by photoacoustic imaging using nano-rGO as a photoacoustic contrast agent (Fig. 10).

Patel *et al.* reported enhanced photoacoustic effect of less oxygenated nanosize graphene.[129] They synthesized nanosize graphene by microwave heating of graphite in a mixture of nitric acid and sulfuric acid without adding $KMnO_4$. By excluding the strong oxidant, these authors obtained nanosize graphene with smaller number of oxygen functional groups. Obtained nanographene shows a small lateral size (~ 10 nm) and can be easily dispersed in water with higher absorption in the NIR (700 nm ~ 1.3 μm), implying that the larger sp^2 domains existed in the product. The reason for dispersibility of such nanographene could be attributed to the small size, so that covering the poor soluble domains required fewer functional groups at the edge compared with its larger-size counterpart, the rGOs. As a result, the synthesized nanographene exhibited respectable photoacoustic wave generation.

6.2 Magnetic resonance Imaging (MRI)

MRI is a very powerful tool for imaging the nervous system, cardiac system, and tumors.[130] The lattice-spin (longitudinal) relaxation time T_1 and spin-spin (transverse) relaxation time T_2 of water proton's magnetic moment are environment-dependent.[131] Therefore, in principle, MRI can be used for differentiating pathological tissues from healthy tissues in non-invasive manner. Yet, practically, some diseases do not yield distinctive relaxation times, and the corresponding tissue is inaccessible to MRI imaging. To diagnose these inaccessible pathological tissues, MRI contrast agents should be introduced for enhancing the relaxation time difference. Most frequently used and commercialized MRI contrasts are paramagnetic metal ion complexes and paramagnetic nanoparticles.[132] Because graphene does not possess intrinsic paramagnetism, graphene itself cannot serve as an MRI contrast agent. However, high density of oxygenated functional groups and cavities in GOs can be used to retain the drugs with conventional MRI contrasts, and their readily functionalized edges enable the targeting ability simultaneously. In addition, anchoring the MRI contrasts on GOs may mitigate the toxicity of heavy metal ion contrast agents due to the decreased release rate. Thus, GOs can be employed as a decent platform for developing novel multifunctional MR imaging agents.

6.2.1 Paramagnetic ions coordinated graphene

Ions of paramagnetic metals including gadolinium (Gd), manganese (Mn), and iron (Fe) have high magnetic moments. Thus, spin-lattice relaxation occurs efficiently when water molecules are coordinated on these ions. Because decreased net magnetization with time can contribute to the T_1 contrast, metal ions with high magnetic moments can be used as T_1 contrast agents.[131] However, highly paramagnetic metal ions are generally toxic owing to the non-selective coordination with biomolecules. Thus, chelated forms are generally used as contrast agents.[132] Graphene, with many oxygenated functional groups and cavities, can be readily coordinated with the metal ions by chelation or burying the ions between graphene layers.

Gizzatov *et al.* used graphene nanoribbons (GNRs) for Gd^{3+} ions coordination.[133] Multi-walled carbon nanotubes (MWCNTs) were reductively cut using K/Na alloy, and functionalized with *p*-carboxyphenyldiazonium salt to produce highly carboxylated GNRs of several nanometer scale (125-280 nm in width and 7-15 nm in thickness). Thus, Gd^{3+} ions were coordinated with GNRs without any surfactants, forming Gd/GNRs. Relaxation rates of T_1 and T_2 were determined per Gd^{3+} concentration at 1.41 T, yielding $r_1 = 70 \pm 6$ $mM^{-1}s^{-1}$ and $r_2 = 108 \pm 9$ $mM^{-1}s^{-1}$. T_1-weighted and T_2-weighted phantom images clearly exhibiting Gd^{3+}-coordinated GNRs produced better MRI contrasts than those obtained with GNRs or H_2O alone.

On the other hand, Kanakia *et al*. intercalated Mn^{2+} ions in the dextran-coated graphene nanoplatelets (GNP-Dex) for T_1-weighted MRI contrasts.[134] The intercalated Mn^{2+} ions were stable in GNP-Dex nanoparticles at the physiological temperature, and thus could be used as clinical MRI contrasts. The relaxation rate was determined per manganese ion concentration, and the obtained slope was $r_1 = 92.2$ $mM^{-1}s^{-1}$. In addition, enhanced T_1-weighted phantom image owing to the high r_1 relaxivity suggests that Mn^{2+}-intercalated GNP-Dex can serve as a good MRI contrast.

6.2.2 Paramagnetic nanoparticles decorated graphene

Commercially available nanoparticle-based MRI contrast agents are usually based on magnetic iron oxides such as the super-paramagnetic iron oxide (SPIO).[135] The relaxation mechanism in super-paramagnetic clusters differs from that in the paramagnetic ions. The large magnetic field around a paramagnetic nanoparticle induces dephasing of water molecule spins near the nanoparticle, yielding transverse relaxation T_2 contrast. Because the nanoparticles can be directly grown on graphene or capped ligands can be linked with graphene, paramagnetic nanoparticles can be easily combined for producing graphene-based T_2 contrast agents.

The first attempt to use a graphene-based T_2 contrast agent was reported in 2011 by Chen *et al.*[136] Fe_3O_4 nanoparticles coated with DMSA were synthesized and covalently bonded with aminodextran (AMD), followed by EDC coupling with GOs to make a Fe_3O_4-GO composite. The size of Fe_3O_4-GO was 174.4 nm in average, determined by dynamic light scattering (DLS). The saturated magnetizations of the materials were 14, 11.5, 7.3 emu g^{-1} for DMSA-Fe_3O_4, AMD-Fe_3O_4, and GO-Fe_3O_4. The T_2 relaxation rate as a function of Fe concentration of Fe_3O_4-GO was higher ($r_2 = 76$ mM^{-1} s^{-1}) than the others (r_2 (DMSA-Fe_3O_4) = 24 mM^{-1} s^{-1}, r_2 (AMD-Fe_3O_4) = 21 mM^{-1} s^{-1}), indicating that aggregation of magnetic particles on GOs enhances the T_2 contrast. Shi *et al.* reported iron oxide nanoparticles (IONPs) decorated GOs for MRI contrast agent.[137] IONPs were adsorbed on the surface of GO, followed by Au nanoparticle (AuNP) growth and PEG functionalization to make IONPs and AuNPs decorated GO complex (IONP-GO-Au), and the average size fell between 200 and 600 nm. Obtained graphene-based material showed strong paramagnetic characteristic originated from IONPs, and T_2-weighted image clearly differentiated the tumor region (Fig. 11). Other types of paramagnetic nanoparticles could also be combined by employing a similar method. Manganese ferrite ($MnFe_2O_4$) nanoparticle-GO composite yielded T_2 relaxation ($r_2 = 256.2$ Fe mM^{-1} s^{-1}),[138] and needle-shaped β-FeOOH nanorods exhibited the highest T_2 relaxation ($r_2 = 303.82$ Fe mM^{-1} s^{-1}) when combined with GO.[139]

6.2.3 Graphene-based multifunctional MRI agents

Multifunctional materials for theranostics have recently attracted a number of researchers' interests because efficient therapy can be achieved by combining imaging, targeting and curing desirably. In the case of graphene derivatives, abundant functionality features enable potentially high loading capacity of drugs, and low toxicity makes them promising multifunctional platform candidates.

Wang *et al*. reported graphene-based multifunctional probes by combining magnetic graphene and mesophorous silica nanosheets.[140] Fe_3O_4 nanoparticle-decorated graphene was coated with tetraethyl orthosilicate (TEOS) and aminopropyltriethoxysilane (APTES), followed by coupling with interleukin-13-based peptide (IP) and doxorubicin (DOX). The average size of graphene based silica probes was 200 nm, and the size of grown Fe_3O_4 nanoparticles was 4-15 nm. T_2-weighted magnetic resonance imaging of intravenously injected PEG conjugated nanocarrier (MGMSP) and additional IP conjugated nanocarrier (MGMSPI) demonstrated that the targeting ability was originated by IP. The DOX loading capacity of the IP-conjugated magnetic graphene-mesophorous silicate (MGMSPID) reached 0.95 μg/μg with 43.19 % loading efficiency, and *in vitro* DOX release by photothermal heating revealed that loaded DOX could be easily desorbed with high concentration of hydrogen ions at high temperature due to the weakened electrostatic and hydrophobic interactions. Similarly, another type of anticancer drug, 5-FU, could be loaded on the Fe_3O_4 nanoparticle/GO composite.[141]

7. Perspectives and future applications

The promising aspects of graphene derivatives for imaging applications are: availability to produce various forms of graphene derivatives for different imaging techniques, high

dispersibility upon conjugating diverse molecules and possibility to deliver drugs with specific targeting ability. The strong intrinsic Raman scattering signals can be utilized for Raman imaging, and increased NIR absorbance of reduced version of derivatives is advantageous for successful photoacoustic imaging. The fluorescence characteristics of GOs and GQDs can be tuned by modifying functional groups, and enhanced QY makes fluorescence imaging another plausible method. Although CNTs have useful optical properties and have been considered for biological applications early on, the difficult separation steps may hinder large-scale production of well-defined CNTs. On the other hand, the dispersed forms of graphene are more applicable to mass production. Solvothermal synthesis employing sodium had already achieved gram-scale graphene,[142] and shear exfoliation in NMP can be readily used in industry-scale production.[143] In addition, in contrast to the CNTs, graphene does not require further purification steps, which present a hurdle for CNTs commercialization. Produced graphene can be further oxidized under oxidative condition for introducing additional oxygenated functional groups, and functional ligands and biomolecules can be incorporated for increasing graphene's water dispersibility and targeting, which is desired for bio-imaging.

For more advanced analysis, multiplex diagnosis and imaging are crucial for in *vivo* experiments. Multiplex analysis can be achieved with CNMs' intrinsic narrow and tunable Raman scattering peaks as the Dai group multiple target imaging with SWNTs. The strategy was to couple different targeting ligands to CNTs with different C12/C13 compositions, because their vibrational frequency was red-shifted by the mass change, altering the Raman peaks of the CNTs.[144] Graphene has not been employed for multiple target imaging with Raman microscopy, but as demonstrated from the studies with CNTs, alteration of isotope composition for multicolor imaging is expected to be exploited in the near future.

Among many graphene derivatives, CVD graphene exhibits high electron conductivity and fast heat dissipation. Low density of defects could serve to perfectly trap liquid for preventing vaporization in high vacuum or ultra-high vacuum conditions, which are the mandatory conditions for electron microscopy analysis. Thus, graphene can be utilized as an atomically thin window for *in situ* electron microscopy for liquid state samples, including various biomolecules and tissues. In addition, this single-atom thick film would make conformal contacts with non-conductive samples assuring the details of surface information. Thus, it could be employed as a novel conductive coating material for scanning electron microscopy (SEM) analysis where noble metals such as platinum (Pt) are currently used.

8. Conclusions

In this review, we highlighted recent applications of graphene-based nanomaterials as versatile imaging tools. As mentioned, graphene has exceptional optical properties for fluorescence imaging: resistance to photobleaching, low toxicity, tunable emission wavelength. In addition, various forms of graphene also possess other remarkable properties including high Raman scattering intensity, large absorption cross section in the NIR region, sharp photoacoustic contrast with NIR incident beam, which all are essential properties for bio-imaging. In addition, diverse organic molecules and biomolecules can be easily conjugated with these graphene derivatives. Based on the status of current research, we expect graphene-based nanomaterials will play vital roles in a number of important imaging studies in the near future.

Acknowledgements

B. H. H. acknowledges financial support from the Global Research Lab (GRL) Program (2013-056425), and the Global Frontier R&D Program on Centre for Advanced Soft Electronics (20110031629) through the National Research Foundation of Korea funded by the Ministry of Science, ICT & Future, Korea. The student (JMY) is grateful for the financial support by Global PH.D Fellowship Program through the National Research Foundation of Korea (NRF) funded by the Ministry of Education (NRF-2014H1A2A1016534).

Notes and references

[a] Department of Chemistry, Seoul National University (SNU), Seoul 151-747, Korea. Email: byunghee@snu.ac.kr
† These authors contributed equally to this work.

1 K. S. Novoselov, A. K. Geim, S. V. Morozov, D. Jiang, Y. Zhang, S. V. Dubonos, I. V. Grigorieva and A. A. Firsov, *Science*, 2004, **306**, 666.
2 A. K. Geim and K. S. Novoselov, *Nat. Mater.*, 2007, **6**, 183.
3 C.-H. Lu, H.-H. Yang, C.-L. Zhu, X. Chen and G.-N. Chen, *Angew. Chem. Int. Ed.*, 2009, **48**, 4785.
4 J.-J Liu, X.-L Zhang, Z.-X Cong, Z.-T Chen, H.-H Yang and G.-N Chen, *Nanoscale*, 2013, **5**, 1810.
5 Y. Wang, L. Zhang, R.-P Liang, J.-M Bai, and J.-D Qiu, *Anal. Chem*. 2013, **85**, 9148
6 X. Li, S. Zhu, B. Xu, K. Ma, J. Zhang, B. Yang and W. Tian, *Nanoscale*, 2013, **5**, 7776
7 S.-J. Jeon, S.-Y. Kwak, D. Yim, J.-M Ju, and J.-H Kim, *J. Am. Chem. Soc,*. 2014, **136**, 10842
8 Q. Mei, C. Jiang, G. Guan, K. Zhang, B. Liu, R. Liu and Z. Zhang, *Chem. Commun.*, 2012, **48**, 7468.
9 W. C. Lee, C. H. Y. X. Lim, H. Shi, L. A. L. Tang, Y. Wang, C. T. Lim and K. P. Loh, *ACS Nano*, 2011, **5**, 7334.
10 S. Y. Par, J. Par, S. H. Sim, M. G. Sung, K. S. Kim, B. H. Hong and S. Hong, *Adv. Mater.*, 2011, **23**, H263.
11 J. T. Robinson, S. M. Tabakman, Y. Liang, H. Wang, H. S. Casalongue, D. Vinh and H. Dai, *J. Am. Chem. Soc.*, 2011, **133**, 6825.
12 B. Tian, C. Wang, S. Zhang, L. Feng and Z. Liu, *ACS Nano*, 2011, **5**, 7000.
13 S. Abhishek, W. I. Choi, J. H. Lee, G. Tae, *Biomaterials,* 2013, **34**, 6239.
14 L. Zhou, L. Zhou, S. Wei, X. Ge, J. Zhou, H. Jiang, F. Li, J. Shen, *J. Photochem. Photobio B*, 2014, **135**, 7.

15 B. Tian, C. Wang, S. Zhang, L. Feng, and Z. Liu, *ACS Nano*, 2011, **5**, 7000.
16 H. Kim and W. J. Kim, *Small*, 2014, **10**, 117.
17 P. Matteini, F. Tatini, L. Cavigli, S. Ottaviano, G. Ghini and R. Pini, *Nanoscale*, 2014, **6**, 7947.
18 V. S.hanmugam, S. Selvakumar and C.-S. Yeh, *Chem. Soc. Rev.*, 2014, **43**, 6254.
19 D. Pan, J. Zhang, Z. Li and M. Wu, *Adv. Mater*., 2010, **22**, 734.
20 T. Gokus, R. R. Nair A. Bonetti, M. Böhmler, A. Lombardo, K. S. Novoselov, A. K. Geim, A. C. Ferrari and A. Hartschuh, ACS Nano, 2009, **3**, 3963.
21 Y. Li, Y. Zhao, H. Cheng, Y. Hu, G. Shi, L. Dai and L. Qu, J. Am. Chem. Soc., 2012, **134**, 15..
22 G. Eda, Y.-Y. Lin, C. Mattevi, H. Yamaguchi, H.-A. Chen, I-S. Chen, C.-W. Chen and M. Chhowalla, *Adv. Mater.*, 2010, **22**, 505.
23 H. Tetsuka, R. Asahi, A. Nagoya, K. Okamoto, I. Tajima, R. Ohta and A. Okamoto, *Adv. Mater*., 2012, **24**, 5333.
24 M. A. Sk, A. Ananthanarayanan, L. Huang, K. H. Lim and P. Chen, *J. Mater. Chem. C*, 2014, **2**, 6954.
25 E. Morales-Narváez and A. Merkoçi, *Adv. Mater.*, 2012, **24**, 3298.
26 C.-T. Chien, S.-S. Li, W.-J. Lai, Y.-C. Yeh, H.-A. Chen, I.-S. Chen, L.-C. Chen, K.-H. Chen, T. Nemoto, S. Isoda, M. Chem, T. Fujita, G. Eda, H. Yamaguchi, M. Chhowalla and C.-W. Chen, *Angew. Chem. Int. Ed.,* 2012, **51**, 6662.
27 L. J. Cote, R. Cruz-Silva, J. X. Huang, *J. Am. Chem. Soc.*, 2009, **131**, 11027.
28 Q. Mei, K. Zhang, G. Guan, b. Liu, S. Wang and Z. Zhang, *Chem. Commun*, 2010, **46**, 7319.
29 A. C. Ferrari and D. M. Basko, *Nat. Nanotechnol.*, 2013, **8**, 235.
30 L. M. Malard, M. A. Pimenta, G. Dresselhaus and M. S. Dresselhaus, *Phys. Rep.*, 2009, **473**, 51.
31 K. N. Kudin, B. Ozbas, H. C. Schniepp, R. K. Prud′homme, I. A. Aksay and R. Car, *Nano Lett.*, 2008, **8**, 36.45
32 F. Schedin, E. Lidorikis, A. Lombardo, V. G. Kravets, A. K. Geim, A. N. Grigorenko, K. S. Novoselov and A. C. Ferrari, *ACS Nano*, 2010, **4**, 5617.
33 S. Sun and P. Wu, *Phys. Chem. Chem. Phys.*, 2011, **13**, 21116.
34 L. V. Wang, *IEEE J. Sel. Top. Quantum Electron.*, 2008, **14**, 171.
35 K. P. Loh, Q. Bao, G. Eda and M. Chhowalla, *Nat. Chem.*, 2010, **2**, 1015.
36 X. Sun, Z. Liu, K. Welsher, J. T. Robinson, A. Goodwin, S. Zaric and H. Dai, *Nano Res*., 2008, **1**, 203.
37 Z. Liu, J. T. Robinson X. M. Sun and H., *Chem. Soc. Rev.*, 2013, **42**, 530.
38 S. Zhu, H. Zhen, Y. Li, P. Wang, X. Huang and P. Shi, *J. Nanopart. Res.*, 2014, **16**, 2530.
39 P. S. Wate, S. S. Banerjee, A. Jalota-Badhwar, R. R. Mascarenhas, K. R. Zope, J. Khandare and R. D. K. Misra, *Nanotechnology*, 2012, **23**, 415101.
40 S. A. Zhang, K. Yang, L. Z. Feng and Z. Liu,, *ACS Nano*, 2011, **49**, 4040.
41 G. Gollavelli and Y.-C. Ling, *Biomaterials*, 2012, **33**, 2532.
42 C. Peng, W. Hu, Y. Zhou, C. Fan and G. Huang, *Small*, 2010, **6**, 1686.
43 K. Yang, S. Zhang, G. Zhang, X. Sun, S.-T. Lee and Z. Liu, *Nano Lett*., 2010, **10**, 3318.
44 M.-L. Chen, J.-W. Liu, B. Hu, M.-L. Chen and J.-H. Wang, *Analyst*, 2011, **136**, 4277.
45 K. Yang, J. Wan, S. Zhang, B. Tian, Y. Zhang and Z. Liu, *Biomaterials*, 2012, **33**, 2206.
46 S.-H Hu, Y.-W. Chen, W.-T. Hung, I.-W. Chen and S.-Y. Chen, *Adv. Mater*, 2012, **24**, 1748.
47 B. Tian, C. Wang, S. Zhang, L. Feng and Z. Liu, *ACS Nano*, 2011, **5**, 7000.
48 M.-L. Chen, Y.-J. He, X.-W. Chen and J.-H. Wang, *Bioconjugate Chem.*, 2013, **24**, 387.
49 J.-L. Li, H.-C. Bao, X.-L. Hou, L. Sun, X.-G. Wang and M. Gu, *Angew. Chem. Int. Ed.*, 2012, **51**, 1830.
50 A.-A. Nahain, J.-E. Lee, J. H. Jeong and S. Y. Park, *Biomacromolecules.*, 2013, **14**, 4082.
51 X. Mao and H. Li, *J. Mater. Chem. B*, 2013, **1**, 4267.
52 Z. Sun, P. Huang, G. Tong, J. Lin, A. Jin, P. Rong, L. Zhu, L. Nie, G. Niu, F. Cao and X. Chen, *Nanoscale*, 2013, **5**, 6857.
52 H. Hong, K. Yang, Y. Zhang, J. W. Engle, L. Feng, Y. Yang, T. R. Nayak, S. Goel, J. Bean, C. P. Theuer, T. E. Barhar, Z. Liu and W. Cai, *ACS Nano*, 2012, **6**, 2361.
54 L. Zhang, Y. Xing, N. He, Y. Zhang, Z. Lu, J. Zhang and Z. Zhang, *J. Nanosci. Nanotechnol.*, 2012, **12**, 2924.
55 S. Zhu, J. Zhang, C. Qiao, S. Tang, Y. Li, W. Yuan, B. Li, L. Tian, F. Liu, R. Hu, H. Gao, H. Wei, H. Zhang, H. Cun and B. Yang, *Chem. Commun.*, 2011, **47**, 6858.
56 D. Pan, L. Guo, J. Zhang, C. Xi, Q. Xue, H. Huang, J. Li, Z. Zhang, W. Yu, Z. Chen, Z. Li and M. Wu, *J. Mater. Chem*., 2012, **22**, 3314.
57 M. Zhang, L. Bai, W. Shang, W. Xie, H. Ma, Y. Fu, D. Fang, H. Sun, L. Fan, M. Han, C. Liu and S. Yang, *J. Mater. Chem.*, 2012, **22**, 7461.
58 L.-L. Li, J. Ji, R. Fei, C.-Z. Wang Q. Lu, J.-R. Zhang, L.-P. Jiang and J.-J. Zhu, *Adv. Funct. Mater.*, 2012, **22**, 2971.
59 X. Wu, F. Tian, W. Wang, J. Chen, M. Wu and J. X. Zhao, *J. Mater. Chem. C*, 2013, **1**, 4676.
60 S. Zhu, J. Zhang, S. Tang, C. Qiao, L. Wang, H. Wang, X. Liu, B. Li, Y. Li, W. Yu, X. Wang, H. Sun and B. Yang, *J Adv. Funct. Mater.*, 2012, **22**, 4732.
61 G. K. Ramesha and S. Sampath, *J. Phys. Chem. C*, 2009, **113**, 7985.
62 S. Stankovich, D. A. Dikin, R. D. Piner, K. A. Kohlhaas, A. Kleinhammes, Y. Jia, Y. Wu, S. T. Nguyen and R. S. Ruoff, *Carbon*, 2007, **45**, 1558.
63 S. Shi, K. Yang, H. Hong, H. F. Valdovinos, T. R. Nayak, Y. Zhang, C. P. Theuer, T. E. Barnhart, Z. Liu and W. Cai, *Biomaterials*, 2013, **34**, 3002.
64 K. Liu, J.-J. Zhang, F.-F. Cheng, T.-T. Zheng, C. Wang and J.-J. Zhu, *J. Mater. Chem.*, 2011, **21**, 12034.
65 Z. Sheng, L. Song, J. Zheng, D. Hu, M. He, M. Zheng, G. Gao, P. Gong, P. Zhang, Y. Ma and L. Cai, *Biomaterials*, 2013, **34**, 5236.
66 U. Resch-Genger, M. Grabolle, S. Cavaliere-Jaricot, R. Nitschke and T. Nann, *Nat. Methods*, 2008, **5**, 763.
67 S. J. Soenen, J. Demeester, S. C. de Smedt, K. Braeckmans, *Biomaterials*, 2012, **33**, 4882.
68 A. M. Derfus, W. C. W. Chan and S. N. Bhatia, *Nano Lett.*,2004, **4**, 11.

69 C. Kirchner, T. Liedl, S. Kudera, T. Pellegrino, A. M. Javier, H. E. Gaub, S. Sto1lzle, N. Fertig and W. J. Parak, *Nano Lett*., 2005, **5**, 331.
70 N. Chen, Y.He, Y. Su, X. Li, Q. Huang, H. Wang, X. Zhang, R. Tai and C. Fan, *Biomaterials*, 2012, **33**, 1238.
71 S. J. Cho, D. Maysinger, M. Jain, B. Röder, S. Hackbarth and F. M. Winnik, *Langmuir*, 2007, **23**, 1974.
72 M. Bottrill and M. Green, *Chem. Commun.*, 2011, **47**, 7039.
73 J. R. Burns, N. Al-Juffali, S. M. Janes, and S. Howorka, *Angew. Chem. Int. Ed*., 2014, **53**, 12466.
74 H. Wang, S.-T. Yang, A. Cao, and Y. Liu, *Acc. Chem. Res.*, 2013, **46**, 750.
75 K. Yang, J. Wan, S. Zhang, Y. Zhang, S.-T. Lee, and Z. Liu, *ACS Nano*, 2011, **5**, 516.
76 M. Nurunnabi, Z. Khatun, K. M. Huh, S. Y. Park, D. Y. Lee, K. J. Cho and Y.-K. Lee, *ACS Nano*, 2013, **7**, 6858.
77 K. Yang, H. Gong, X. Shi, J. Wan, Y. Zhang, Z. Liu, *Biomaterials*, 2013, **34**, 2787.
78 Y. Chong, Y. Ma, H. Shen, X. Tu, X. Zhou, J. Xu, J. Dai, S. Fan and Z. Zhang, *Biomaterials*, 2014, **35**, 5041.
79 S. J. Soenen, J. Demeester, S. C. de Smedt, K. Braeckmans, *Biomaterials*, 2012, **33**, 4882.
80 A. M. Derfus, W. C. W. Chan and S. N. Bhatia, *Nano Lett.*,2004, **4**, 11.
81 X. T. Zheng, A. Than, A. Ananthanaraya, D.-H. Kim and P. Chen, *ACS Nano*, 2013, **7**, 6278.
82 Y. Liu, Y. Zhao, B. Sun, and C. Chen, *Acc. Chem. Res.*, 2013, **46**, 702.
83 F. Guo, N. Ma, Y. Horibe, S. Kawanishi, M. Murata, Y. Hiraku, *Toxicol. Appl. Pharm.*, 2012, **260**, 183.
84 H. K. Lindberga, G. C.-M. Falcka, R. Singhc, S. Suhonena, H. Järventaus, E. Vanhala, J. Catalána, P. B. Farmer, K. M. Savolainena, H. Norppa, *Toxicology*, 2013, **313**, 24.
85 K. Shimizu, A. Uchiyama, M. Yamashita, A. Hirose, T. Nishimura and N. Oku, *J. Toxicol. Sci*., 2013, **38**, 7.
86 X. Huang, F. Zhang, X. Sun, K. Y. Choi, G. Niu, G. Zhang, J. Guo, S. Lee, and X. Chen, *Biomaterials*, 2014, **35**, 856.
87 G. P. Kotchey, S. A. Hasan, A. A. Kapralov, S. H. Ha, K. Kim, A. A. Shvedova, V. E. Kagan, and A. Star, *Acc. Chem. Res.*, 2012, **45**, 1770.
88 S. Liu, L. Wei, L. Hao, N. Fang, M. W. Chang, R. Xu, Y. Yang, and Y. Chen, *ACS Nano*, 2009, **3**, 3891.
89 S. K. Sohaebuddin, P. T Thevenot, D. Baker, J. W. Eaton, L. Tang, *Part. Fibre, Toxicol*., 2010, **7**, 22.
90 A. M. Jastrzebska, P. Kurtycz, A. R. Olszyna, *J Nanopart Res.*, 2012, **14**, 1320
91 C. Fisher, A. E. Rider, Z. J. Han, S. Kumar, I. Levchenko, and K. Ostrikov, *J. Nanomater.*, 2012, **2012**, 315185.
92 A. Sasidharan, L. S. Panchakarla, P. Chandran, D. Menon, S. Nair, C. N. R. Raob and M. Koyakutty, *Nanoscale*, 2011, **3**, 2461.
93 C. Wu, C, Wang, T. Han, X. Zhou, S. Guo and J. Zhang, *Adv. Healthcare Mater.*, 2013, **2**, 1613.
94 H. Zhang, C. Peng, J. Yang, M. Lv, R. Liu, D. He, C. Fan and Q. Huang, *ACS Appl. Mater. Interfaces*, 2013, **5**, 1761.
95 X. Yuan, Z. Liu, Z. Guo, Y. Ji, M. Jin and X. Wang, *Nanoscale Res Lett.*, 2014, **9**, 108
96 K. Wang, J. Ruan, H. Song, J. Zhang, Y. Wo, S. Guo, D. Cui, *Nanoscale Res Lett.*, 2011, **6**, 1.
97 A. Schinwald, F. A. Murphy, A. Jones, W. MacNee, and K. Donaldson, *ACS Nano*, 2012, **6**, 736.
98 S. M. Chowdhury, G. Lalwani, K. Zhang, J. Y. Yang, K. Neville and B. Sitharaman, *Biomaterials*, 2013, **34**, 283.
99 L. De Marzi, L.Ottaviano, F. Perrozzi, M. Nardone, S. Santucci, J. De Lapuente, M. Borras, E. Treossi, V. Palermo, A. Poma, *J. Biol. Reg. Homeos. Ag*. 2014, **28**, 281.
100 O. Akhavan, E. Ghaderi, A. Akhavan, *Biomaterials*, 2012, **33**, 8017
101 O. Akhavan and E. Ghaderi, *ACS Nano*, 2010, **4**, 5731
102 W. Kong, J. Liu, R. Liu, H. Li, Y. Liu, H. Huang, K. Li, J. Liu, S.-T. Lee and Z. Kang, *Nanoscale*, 2014, **6**, 5116.
103 L. Yan, F. Zhao, S. Li, Z. Huc and Y. Zhao, *Nanoscale*, 2011, **3**, 362
104 G. P. Kotchey, B. L. Allen, H. Vedala, N. Yanamala, A. A. Kapralov, Y. Y. Tyurina, J. Klein-Seetharaman, V. E. Kagan, and A. Star, *ACS Nano,* 2011, **5**, 2098.
105 J. Zhang, R. E. Campbell, A. Y. Ting and R. Y. Tsien., *Nat Rev Moll Cell Bio*., 2002, **3**, 906.
106 A.-A. Nahain, J.-E. Lee, I. In, H. Lee, K. D. Lee, J. H. Jeong, and S. Y. Park, *Mol. Pharmaceutics*, 2013, **10**, 3736.
107 J. Ge, M. Lan, B. Zhou, W. Liu, L. Guo, H. Wang, Q. Jia, G. Niu, X. Huang, H. Zhou, X. Meng, P. Wang, C.-S. Lee, W. Zhang and X. Han, *Nat. Commun.,* 2014, **5**, 4596.
108 J. Qian, D. Wang, F.-H. Cai, W. Xi, L. Peng, Z.-F. Zhu, H. He, M.-L. Hu and S. He, *Angew. Chem. Int. Ed.*, 2012, **51**, 10570.
109 Q. Liu, B. Guo, Z. Rao, B. Zhang and J. Ru Gong, *Nano Lett.*, 2013, **13**, 2436.
110 S. Keren, C. Zavaleta, Z. Cheng, A. de la Zerda, O. Gheysens and S. S. Gambhir., *Proc. Natl. Acad. Sci. U.S.A.*, 2008, **105**, 5844.
111 X. M. Qian, X. H. Peng, D. O. Ansari, Q. Yin-Goen, G. Z. Chen, D. M. Shin, L. Yang, A. N. Young, M. D. Wang and S. M. Nie, *Nat. Biotechnol.*, 2008, **26**, 83.
112 Z. Liu, X. Li, S. M. Tabakman, K. Jiang, S. Fan and H. Dai, *J. Am. Chem. Soc.*, 2008, **130**, 13540.
113 C. L. Zavaleta, A. de la Zerda, Z. Liu, S. Keren, Z. Cheng, M. Schipper, X. Chen, H. Dai and S. S. Gambhir, *Nano Lett.*, 2008, **8**, 2800.
114 C. L. Zavaleta, B. R. Smith, I. Walton, W. Doering, G. Davis, B. Shojaei, M. J. Natan and S. S. Gambhir, *Proc. Natl. Acad. Sci. U.S.A.*, 2009, **106**, 13511.
115 Z. Zhang, F. Xu, W. Yang, M. Guo, X. Wang, B. Zhang and J. Tang, *Chem. Commun.*, 2011, **47**, 6440.
116 Y. Yang, C. He, W. He, L. Yu, R. Peng. X. Xie, X. Wang and Y. Mai, *J. Nanopart. Res.*, 2011, **13**, 5571.
117 Y. H. Lee, L. Polavarapu, N. Gao, P. Yuan and Q.-H Xu, *Lagmuir*, 2011, **28**, 321.
118 Q. Liu, L. Wei, J. Wang, F. Peng, D. Luo, R. Cui, Y. Niu, X. Qin, Y. Liu, H. Sun, J. Yang, and Y. Li, *Nanoscale*, 2012, **4**, 7084.
119 J. Huang, C. Zong, H. Shen, M. Liu, B. Chen, B. Ren, and Z. Zhang, *Small*, 2012, **8**, 2577.
120 X. Ma, Q. Qu, Y. Zhao, Z. Luo, Y. Zhao, K. W. Ng, and Y. Zhao, *J. Mater. Chem. B*, 2013, **1**, 6495.
121Z. Liu, Z. Guo, H. Zhong, X. Qin, M. Wan, and B. Yang, *Phys. Chem. Chem. Phys.*, 2013, **15**, 2961.
122 V. Ntziachristos, *Nat. Methods*, 2010, **7**, 603.
123 M. Xu and L. V. Wang, *Rev. Sci. Instrum.*, 2006, **77**, 041101.

124 A. de la Zerda, C. Zavaleta, S. Keren, S. Vaithilingam, S. Bodapati, Z. Liu, J. Levi, B. R. Smith, T.-J. Ma, O. Oralkan, Z. Cheng, X. Chen, H. Dai, B. T. Khuri-Yakub and S. S. Gambhir, *Nat. Nanotechnol.*, 2008, **3**, 557.

125 G. Ku and L. V. Wang, *Opt. Lett.*, 2005, **30**, 507.

126 A. Agarwal, S. W. Huang, M. O´Donnell, K. C. Day, M. Day, N. Kotov and S. Ashkenazi, *J. Appl. Phys.*, 2007, **102**, 064701.

127 Y.-W. Wang, Y.-Y. Fu, Q. Peng, S.-S. Guo, G. Liu, J. Li, H.-H. Yang and G.-N. Chen, *J. Mater. Chem. B*, 2013, **1**, 5762.

128 K. Yang , L. Hu , X. Ma , S. Ye , L. Cheng , X. Shi , C. Li , Y. Li and Z. Liu, *Adv. Mater.*, 2012, **24**, 1868.

129 M. A. Patel, H. Yang, P. L. Chiu, D. D. T. Mastrogiovanni, C. R. Flach, K. Savaram, L. Gomez, A. Hemnarine, R. Mendelsohn, E. Garfunkel, H. Jiang and H. He, *ACS Nano*, 2013, **7**, 8147.

130 P. Mansfield, *Angew. Chem. Int. Ed.*, 2004, **43**, 5456.

131 G. J. Strijker, W. J. M. Mulder, G. A. F. van Tilborg and K. Nicolay, *Anticancer Agents Med. Chem.*, 2007, **7**, 291.

132 P. Caravan, J. J. Ellison, T. J. McMurry and R. B. Lauffer, *Chem. Rev.*, 1999, **99**, 2293.

133 A. Gizzatov, V. Keshishian, A. Guven, A. M. Dimiev, F. Qu, R. Muthupillai, P. Decuzzi, R. G. Bryant, J. M. Tour, and L. J. Wilson, *Nanoscale*, 2014, **6**, 3059.

134 S. Kanakia, J. D. Toussaint, S. M. Chowdhury, G. Lalwani, T. Tembulkar, T. Button, K. R. Shroyer, W. Moore, B. Sitharaman, *Int. J. Nanomed.*, 2013, **8**, 2821.

135 H. B. Na, I. C. Song and T. Hyeon, *Adv. Mater.*, 2009, **21**, 2133.

136 W. Chen, P. Yi, Y. Zhang, L. Zhang, Z. Deng, and Z. Zhang, *ACS Appl. Mater. Interfaces*, 2011, **3**, 4085.

137 X. Shi, H. Gong, Y. Li, C. Wang, L. Cheng and Z. Liu, *Biomaterials*, 2013, **34**, 4786.

138 E. Peng, E. S. G. Choo, P. Chandrasekharan, C.-T. Yang, J. Ding, K.-H. Chuang, and J. M. Xue, *Small*, 2012, **8**, 3620.

139 M.-L. Chen, L.-M. Shen, S. Chen, H. Wang, X.-W. Chen, and J.-H. Wang, *J. Mater. Chem. B*, 2013, **1**, 2582.

140 Y. Wang, R. Huang, G. Liang, Z. Zhang, P. Zhang, S. Yu, and J. Kong, *Small*, 2014, **10**, 109.

141 G. Wang, G. Chen, Z. Wei, X. Dong, M. Qi, *Mat. Chem. Phys*, 2013, **141**, 997.

142 M. Choucair, P. Thordarson and J. A. Stride, *Nat. Nanotechnol.*, 2008, **4**, 30.

143 K. R. Paton *et al*., *Nat. Mater.*, 2014, **13**, 6242.

144 Z. Liu, S. Tabakman, S. Sherlock, X. Li, Z. Chen, K. Jiang, S. Fan and H. Dai, *Nano Res.*, 2010, **3**, 222.